This is an author-deposited version published in: https://sam.ensam.eu
Handle ID: .http://hdl.handle.net/10985/17775

To cite this version :

Belkacem MANSER, Idir BELAIDI, Abderrachid HAMRANI, Farid BAKIR, Sofiane KHELLADI - Performance of hydrodynamic journal bearing under the combined influence of textured surface and journal misalignment: A numerical survey - Comptes Rendus Mécanique - Vol. 347, n°2, p.141-165 - 2019

Performance of hydrodynamic journal bearing under the combined influence of textured surface and journal misalignment: a numerical survey

B. MANSER[1,*], I. BELAIDI[1], A. HAMRANI[1], S. KHELLADI[2] & F. BAKIR[2]

[1] *LEMI., FSI., University of M'hamed Bougara, Avenue de I'indépendance, 35000-Boumerdes, Algeria.*
[2] *DynFluid Lab., Arts et Métiers ParisTech, 151 boulevard de l'Hôpital, 75013-Paris, France.*

[*] Corresponding author : b.manser@univ-boumerdes.dz

Abstract

A wisely chosen geometry of micro textures with the favorable relative motion of lubricated surfaces in contacts can enhance tribological characteristics, in this paper, a computational investigation related to the combined influence of bearing surface texturing and journal misalignment on the performances of hydrodynamic journal bearings is reported. To this end, a numerical analysis is performed to test three texture shapes: square "SQ", cylindrical "CY" and triangular "TR", and shaft misalignment variation in angle and degree. The Reynolds equation of thin viscous film is solved using finite differences scheme and mass conservation algorithm (JFO boundary conditions), taking into account the presence of textures on both full film and cavitation regions. Preliminary results are compared with benchmark data and are consistent with a positive enhancement in misaligned bearing performances (load carrying capacity and friction). The results suggest that the micro-step bearing mechanism is a key parameter, where the micro-pressure recovery action present in dimples located at the second angular part of the bearing (from 180° to 360°) can compensate the loss on performances caused by shaft misalignment, while the micro-pressure drop effect at the full film region causes poor performances. Considering the right arrangement of textures on the contact surface, their contours geometries can have a significant impact on the performance of misaligned journal bearings, particularly at high eccentricity ratios, high misalignment degrees and when the misalignment angle α approaches to 0° or 180°.

Keywords: Hydrodynamic journal bearing, JFO boundary conditions, Misalignment effect, Surface texturing, Dimple shapes.

1 Introduction

With the technological progress that has been achieved in recent years, rotating machinery such as electrical motors, generators, pumps, compressors, and high-speed machining spindles, etc., becomes increasingly powerful with higher rotation speed. Hydrodynamic rotor-bearing systems are important parts in present-day heavy machinery. Because of their efficiency, simplicity, high precision, low cost, long life, silent operation, low friction and wear and good heat dissipation [1], bearing systems are widely used in rotor systems and they usually correspond to the best existing technological designs in some rotating machines. One of the most commonly used industrial bearings are the radial-loaded hydrodynamic journal bearings, required to support heavy loads at high rotational speeds. However, they present the most important power losses in rotating machines [2]. It is well known that the misalignment is a disturbing factor that affects directly the operating conditions of journal bearings. Indeed, misalignment arise generally from: manufacturing tolerances, assembly errors, asymmetric bearing load, deflection of journal and bearing supports, improper installation and assembly errors, etc. In general, misalignment causes wear and vibration, reduces bearing performances and life, thus leading to the system failure. Understanding the nature of misalignment has been the object of numerous theoretical and experimental studies [3]. The first one was recorded by MCKEE and MCKEE [4], where the influence of journal misalignment on the maximum pressure location was experimentally analyzed. DUBOIS et al. [5] reported that, under misalignment, the pressure distribution becomes asymmetric where the peak was located at the bearing ends. Subsequently, an experimental analysis about the effect of a known misalignment couple and eccentricity ratio on the proprieties of misaligned plain bearings was conducted [6]. Many theoretical studies were also carried out by many researchers in order to examine the effect of misalignment on the characteristics of various bearing systems. We can quote the following research examples for: plain bearings [7, 8], partial bearings [9], gas bearings [10, 11], tilting-pad journal bearing [12, 13], hydrostatic journal bearing [14, 15], two-lobe bearings [16] and three-lobe bearings[17], etc. In recent years, many works were devoted to the analysis of the combined effects of misalignment and influencing factors; such as: bearing configuration, groove type and its location [18, 19], cavitation effect [20, 21], thermal effect [22, 23], elastic and thermal deformation [24, 25], porosity effect [26, 27], turbulent effect [28, 29], non-Newtonian lubricants [30, 31] and water-lubricated plain journal bearings [32], etc.

In all the above theoretical studies, the analysis of misalignment was performed based on the assumptions of smooth surface bearings. Most recently, the tribology community has been interested on the effect of surface roughness on the performance of hydrodynamically lubricated contacts. Many works [33, 34, 35, 36] were dedicated to the study of the combined influences of surface roughness and journal misalignment on bearing systems using either CHRISTENSEN stochastic theory of rough surfaces [20] or the average flow theory introduced by PATIR and CHENG [37, 38]. The conclusion was that the combined influence of bearing surface roughness and shaft misalignment is more pronounced at higher eccentricities [33], while others published encouraging results reporting that surface roughness may compensate the decrease in minimum film thickness caused by shaft misalignment [35].

Nowadays, the emphasis has been placed on surface texturing and its effect on the performance characteristics of bearing systems. The idea is similar to the surface roughness, but in the case of surface texturing, the operator intentionally incorporates a well defined dimple shape to obtain the desired tribological characteristics [39]. Moreover, with the development of manufacturing technology, particularly micro-fabrication techniques (laser surface texturing [40], reactive ion etching [41], LIGA process [42], vibro-rolling [43], vibro-mechanical texturing [44] and abrasive jet machining [45]) it is now possible to include textures on contact surfaces. Indeed, surface texturing has proved to be very beneficial in the case of hydrodynamic bearing systems [41], where it improves the load-carrying capacity by providing supplementary hydrodynamic pressure [46] and may acting as lubricant reservoirs to ensure supply in cases of lubricant starvation[47], entrapping wear debris and abrasive particles to prevent severe wear [48] and so reducing friction [49]. The introduction of textures in journal bearings was first initiated by LU and KHONSARI [50], they have presented a series of experimental results to examine the effect of fully and partially textured journal bearings on the Stribeck curve. It was shown that the friction coefficient in fully textured bearing, can be reduced, with an appropriate selection of texture size, depth and density. TALA-IGHIL et al. [51, 52] investigated the effect of spherical and cylindrical shapes on the bearing performance, they used a finite-difference model to solve the two-dimensional Reynolds equation under steady-state conditions by considering Reynolds boundary condition. It was reported that textured surface affected the main bearing characteristics. This impact can have either positive or negative influences on this characteristics depending on the dimple parameters (size, depth, density and distribution). Further, they reported, by means of numerical simulation, that the partial texturing configuration including the texturing of multiple zones has a positive influence on hydrodynamic contact characteristics. KANGO et al. [53], performed an investigation related to the combined effects of viscous heat dissipation and non-Newtonian fluid rheology on textured journal bearing performances. Spherical dimples using classical Reynolds model and mass conserving (proposed by Elrod and Adams [54]). It was found that JFO boundary conditions provide realistic results compared with those obtained by Reynolds boundary conditions. Recently, ZHANG et al. [55] presented a parametric design of texturing surface bearing, with the aim to get the optimal textures distribution and parameters, they reported that, the load capacity of a textured journal bearing may be improved through an appropriate arrangement of textures on the contact surface.

In order to explain the behavior of lubricant inside micro-textured surfaces of mechanical seals, several mechanisms have been proposed. We can cite the following works: "Micro-wedge action" generated by micro-textured features identified by HAMILTON et al. [46] and ANNO et al.[56]. " Inlet roughness" mechanism proposed by TØNDER et al. [57, 58]. "Collective dimple effect" proposed by ETSION and BURSTEIN [59]. "Load support mechanism" of inlet suction observed in OLVER et al. [60] and FOWELL et al. [61] works. And finally, "Balancing wedge action" reported by YAGI and SUGIMURA [62]. Based on these mechanisms, NANBU et al. [63] reported that textures with bottom shapes containing a micro-wedge and/or a micro-step bearing mechanisms tend to increase film thicknesses and pressure lift. While, recently, M.S UDDIN et al. [64] mentioned that texture shapes with convergent (positive) wedge bottom profile offer the best performance, divergent (negative) wedge bottom profile perform the worst. Moreover, they also reported that the dimple shape with micro-step features would be beneficial in reducing the friction.

The above-mentioned works show that, the tribological performances of textured surfaces are very sensitive to the texture mechanism. Indeed, some dimple shapes with micro-wedge and/or micro-step features perform better by increasing the load lifting capacity and lowering the friction force. The added feature in this study is the combination of the influences of surface texturing (full/partial) and journal misalignment (degree/angle) on the performance of hydrodynamic journal bearings, using Elrod's efficient mass conservation algorithm for implementation the JFO boundary conditions.

This paper is organized as follows. Section 2 provides the description of modified Reynolds equation, cavitation boundary condition, governing equations and computational procedure. Section 3 is devoted to numerical results and discussions, which contains the preliminary validation and performance analysis of textured misaligned journal bearing. Finally, our conclusions are given in the last section.

2 Governing equations

2.1 Reynolds equation and ELROD Cavitation Algorithm

In lubrication theory, Reynolds equation of thin viscous fluid films is usually used for the prediction of the pressure distribution. For a Newtonian lubricant in laminar flow with constant viscosity, under the isothermal condition, taking into account assumptions that the bushing is stationary and the axial movement of the shaft is neglected, the steady state Reynolds equation (in Cartesian coordinates), takes the following form:

$$\frac{\partial}{\partial x}\left(\rho\, h^3\, \frac{\partial p}{\partial x}\right)+\frac{\partial}{\partial z}\left(\rho\, h^3\, \frac{\partial p}{\partial z}\right)=6\,\mu\, U\, \frac{\partial\,(\rho\, h)}{\partial x} \tag{1}$$

where, p : lubricant pressure, h : film thickness, μ : dynamic viscosity, ρ : lubricant density and U : shaft speed in x direction.

In full-film zone, the density is constant and equation (1) becomes:

$$\frac{\partial}{\partial x}\left(h^3 \frac{\partial p}{\partial x}\right)+\frac{\partial}{\partial z}\left(h^3 \frac{\partial p}{\partial z}\right)=6\,\mu\, U\, \frac{\partial h}{\partial x} \tag{2}$$

In rupture zone, the pressure remains constant at the cavitation pressure. Hence, equation (1) is reduced to:

$$\frac{\partial}{\partial x}\left(\frac{\rho\, h U}{2}\right)=0 \tag{3}$$

In order to take into account the effect of film rupture and reformation, JAKOBSSON, FLOBERG [65] and OLSSON [66] proposed the so-called JFO boundary conditions. The JFO boundary condition have been added to be more realistic then Reynolds boundary condition and sufficiently accurate model to account for lubricant cavitation, especially in: misaligned, dynamical-loaded and textured bearings [20, 22, 23, 67, 53].

To use the JFO boundary conditions, ELROD [54] suggested to combination of the two equations (2) and (3) into a single "universal" equation that covers both the cavitated and the full-film regions, by introducing a new parameter called fractional-film content $\Theta = \rho/\rho_c$, where ρ_c is the cavitated oil density.

The resulting mass conservative form of the Reynolds equation where the unknown is the factional film content instead of the pressure can be written as follows:

$$\frac{\partial}{\partial x}\left(\beta\, h^3\, g\, \frac{\partial \Theta}{\partial x}\right)+\frac{\partial}{\partial z}\left(\beta\, h^3\, g\, \frac{\partial \Theta}{\partial z}\right)=6\,\mu\, U\, \frac{\partial (\Theta\, h)}{\partial x} \tag{4}$$

where β is the bulk modulus which represents the variation of the lubricant compressibility in the full-film region and the pressure p is given by:

$$\beta=\rho\, \frac{\partial p}{\partial \rho} \tag{5}$$

and $g\,(\Theta)$ is the switch function (cavitation index) which is zero in the cavitation zone and equal to unity in the full-film zone.

$$\begin{cases} g=1 & \text{if} \quad \Theta \geq 1 \\ g=0 & \text{if} \quad \Theta < 1 \end{cases} \tag{6}$$

After solving equation (4) for Θ, the pressure in the full-film region can be determined using the following relation [54]:

$$p = p_c + \beta\, g\, \ln(\Theta) \tag{7}$$

where, p_c is the cavitation pressure.
By introducing the following dimensionless parameters:

$$\theta = x/R \quad Z = z/L \quad \overline{h} = h/C \quad \overline{y} = y/h \quad \overline{\beta} = \frac{\beta C^2}{\mu U R}$$

where, R : bearing radius, L : bearing length and C : radial clearance.
The dimensionless form of the modified Reynolds equation becomes:

$$\frac{1}{12}\frac{\partial}{\partial \theta}\left(\overline{\beta}\, g\, \overline{h}^3 \frac{\partial \Theta}{\partial \theta}\right) + \left(\frac{R}{L}\right)^2 \frac{1}{12}\frac{\partial}{\partial Z}\left(\overline{\beta}\, g\, \overline{h}^3 \frac{\partial \Theta}{\partial Z}\right) = \frac{1}{2}\frac{\partial(\Theta \overline{h})}{\partial \theta} \tag{8}$$

and the dimensionless pressure is described by:

$$\overline{P} = \overline{P}_c + \overline{\beta}\, g\, \ln(\Theta) \tag{9}$$

2.2 Film thickness

Oil film thickness “h” is the gap between the journal and the bushing, filled with a liquid lubricant which generate required hydrodynamic pressure. It is one of the most important parameters in Reynolds equation, which needs to be carefully considered in the analysis. Therefore, the Reynolds equation should be modified to allow the variation of film thickness in both directions, taking into account the combined effect of bearing surface texturing and shaft misalignment.

1. Smooth misaligned journal bearing

   In the case of general misaligned conditions, the approach taken from MASPEYROT and FRENE [68] paper is used to represent the oil film thickness distribution inside the bearing with provision for misalignment in both circumferential and axial directions as shown in figure 1.

   $$h_{(\theta,z)} = C + e_0\left(1 + \cos(\theta)\right) + e'\left(\frac{z}{L} - \frac{1}{2}\right)\cos(\theta - \alpha) \tag{10}$$

   where e_0 is the eccentricity at the bearing mid-plane, e' is the magnitude of the projected journal axis on the bearing mid-plane, α is the misalignment angle between the line of centers and the rear center of the misaligned journal (see figure 1).

   The dimensionless film thickness is described by:

   $$\overline{h}_{(\theta,\overline{Z})} = \left(1 + \varepsilon \cos(\theta)\right) + \varepsilon'\left(\overline{Z} - \frac{1}{2}\right)\cos(\theta - \alpha) \tag{11}$$

   the parameters ε is the eccentricity ratio at the bearing mid-plane ($\varepsilon = e_0/C$) and ε' is the misalignment eccentricity ratio, which represent the magnitude of the projection of the complete journal center line on the mid plane, and can be computed from [20]

   $$\varepsilon' = \frac{e'}{C} = D_m\, \varepsilon'_{max} \tag{12}$$

   where D_m the dimensionless degree of misalignment (values from 0 to 1) and ε'_{max} is the maximum possible value of ε', is given by:

   $$\varepsilon'_{max} = 2\left(\sqrt{1 - \varepsilon^2 \sin^2(\alpha)} - \varepsilon\, |\cos(\alpha)|\right) \tag{13}$$

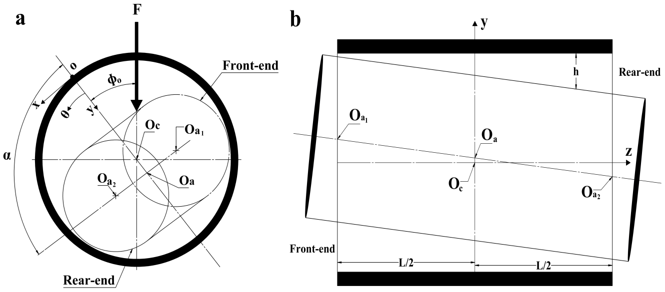

Figure 1: Representative scheme of misaligned journal bearing

2. Textured misaligned journal bearing

   Normalized lubricant film thickness in the case of textured misaligned journal bearing is described by a function of the form:

$$\overline{h}_{T_{(\theta,\overline{Z})}} = \overline{h}_{(\theta,\overline{Z})} + \overline{\Delta h}_{(\theta,\overline{Z})} \tag{14}$$

   where, $\overline{h}_{(\theta,\overline{Z})}$ denotes the smooth part (without textures equation 11) of the film geometry and $\overline{\Delta h}_{(\theta,\overline{Z})}$ is the film thickness variation due to the dimple surface, it characterizes the depth of the fluid film in the texture (Fig 2).

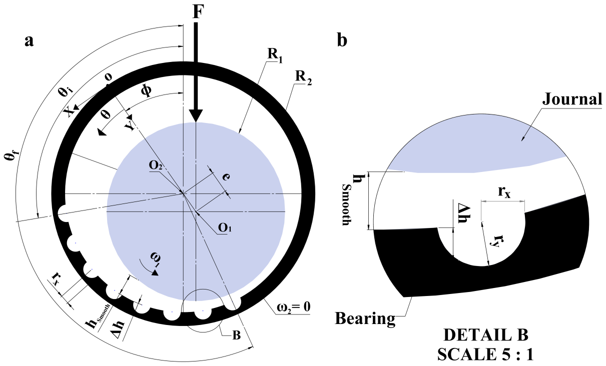

Figure 2: Representative scheme of journal bearing: a) a straight section of the textured journal bearing; b) detailed section for the texture scheme

2.3 Texture shapes and geometries

In general, textures can be characterized by their shape (contour geometry, bottom profile), size (contour dimension, depth), number (along axial/circumferential directions), density and distribution. ZHANG et al. [69] reported that square texture shape performed the best hydrodynamic enhancement, followed by the triangle, circle and rectangle. According to that reasoning, in this study, three texture shapes are adopted: square, cylindrical and triangular to highlight its effect on the particular case of journal bearing. Table 1 summarizes the texture geometries, parameters and equations. The coordinates of the texture center C are noted (x_c, y_c, z_c). This center is located on the bearing surface, making $y_c = 0$. The depth of any point located on the texture geometry is given by $\Delta h_{(x,z)}$. Texture dimensional parameters in the x, y, and z directions, are r_x, r_y , and r_z, respectively.

DE-KRAKER et al. [70] reported that the ratio S between the film thickness h_{min} and the dimple depth r_y is the key texture parameters, they demonstrated that Reynolds equation can be used to investigate the effects of texture when a ratio $S < 1$ exists. According to that reasoning, the following shape dimensions are chosen, $r_x = r_z = 3\,mm$ and $r_y = 0.025\,mm$, where $S = 0.8$.

TALA-IGHIL et al. [52] simulated 25 cases of cylindrical texture shape with different texture distributions including full texturing and partial texturing with one or multiple separated zones of the bearing surface. They reported that, in one side, fully texturing have a detrimental effect, and the partially texturing, in the other side, has a positive influence. Further more, they reported that, optimal region where texturing can provide more efficiency is located at the second half of bearing surface, where the area under the declining part of the pressure field is situated. Due to this, two texture configurations, as shown in figure 3, are considered herein for exploration.

Table 1: Geometric parameters and equations for the studied texture shapes

Description	Square “SQ”	Cylinder “CY”	Triangle “TR”
Texture shapes	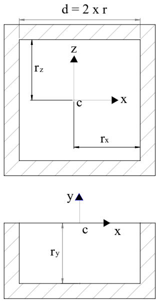	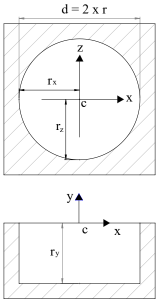	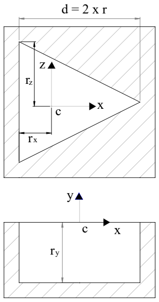
Geometric Equations	if $\begin{cases} -r_x \leq x \leq r_x \\ -r_z \leq z \leq r_z \end{cases}$	if $\begin{cases} r_x = r_z = r \\ (x-x_c)^2 + (z-z_c)^2 = r^2 \end{cases}$	if $\begin{cases} -r_x \leq x \leq r_x \\ \dfrac{r_z}{2r_x} x \leq z \leq -\dfrac{r_z}{2r_x} x + r_z \end{cases}$
	$\Delta h(x,z) = r_y$		

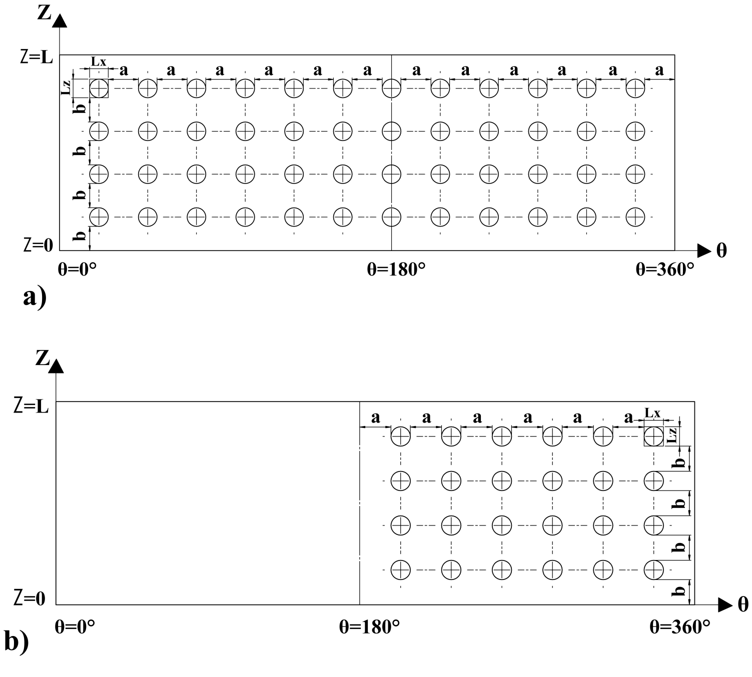

Figure 3: Illustration of textures distribution in the circumferential and axial directions on the bearing surface: a) fully textured cases (from 0° to 360°) ; b) partially textured cases (from 180° to 360°)

2.4 Computational procedure

Based on mass conservation algorithm (JFO boundary conditions), the approach proposed by VIJAYARAGHAVAN and KEITH [71] is used herein. The finite differences method with Gauss-Seidel iterative process (successive over-relaxation "SOR") is employed to compute the fractional film content (Θ). Usually, an iterative loop with a convergence criterion is required when JFO boundary conditions are imposed [67]. Moreover, this method is very easy to implement which makes it the preferred solver for small and medium-sized problems [72]. In order to improve the convergence speed and avoid the problem in stabilizing the cavitation zone, the modified switch function algorithm developed by FESANGHARY and KHONSARI [72] is used in the computational code, where the "gfactor" is chosen from the range of 0 to 0.9.

The computational process consists of :

- Introduction of input data: L/D, ε, D_m and α;
- Input initial values of : fractional film content $\Theta^0_{(\theta,Z)}$, binary switch function $g^0_{(\theta,Z)}$ and film thickness $h^0_{(\theta,Z)}$;
- Solve the modified Reynolds equation (4);
- Imposition of boundary conditions on affected nodes (JFO condition);
- The fractional film content is obtained by verifying the following convergence condition: $\dfrac{|\Delta\Theta_{i,j}|}{\Theta_{i,j}} \leq tol_{\Theta}$ at each node (i,j) of the bearing surface mesh.
- Once the convergence condition is satisfied, the pressure profile can be determined using equation (7) and the bearing characteristics can be deduced.

The process described above corresponds to the resolution of direct problem whose eccentricity ratio ε ,D_m and α are known, for the inverse problem which consist on the determination of the position (the relative position ε , the degree D_m and the angle α of misalignment) of the journal in the bearing for an imposed applied load $\overline{F}$ and moment (magnitude $\overline{M}$ and direction ϕ_M) .

The procedure consists of :

- Input initial values of : the eccentricity ratio ε_0, the degree D_{m_0} and the angle α_0 of misalignment;
- Solve the direct problem for the value of ε_0, $D_{m_0}$and α_0;
- The calculated load-carrying capacity $\overline{W}_C$ is compared with the applied load $\overline{F}$; the calculated misalignment direction ϕ_{M_C} is compared with the applied moment direction ϕ_M and the calculated misalignment moment $\overline{M}_C$ is compared with the applied moment $\overline{M}$;
- Calculation of a new eccentricity ratio ε, new angle of misalignment α and new degree of misalignment D_m by the method of Brent [73];
- The process stopping after the load convergence condition $\dfrac{|\overline{W}_C - \overline{F}|}{\overline{F}} \leq tol_W$; the misalignment angle convergence criteria $|\phi_{M_C} - \phi_M| \leq tol_{\phi_M}$ and the moment convergence condition $\dfrac{|\overline{M}_C - \overline{M}|}{\overline{M}} \leq tol_M$ are satisfied.

We present, the global computational procedure in the following flowchart (figure 4).

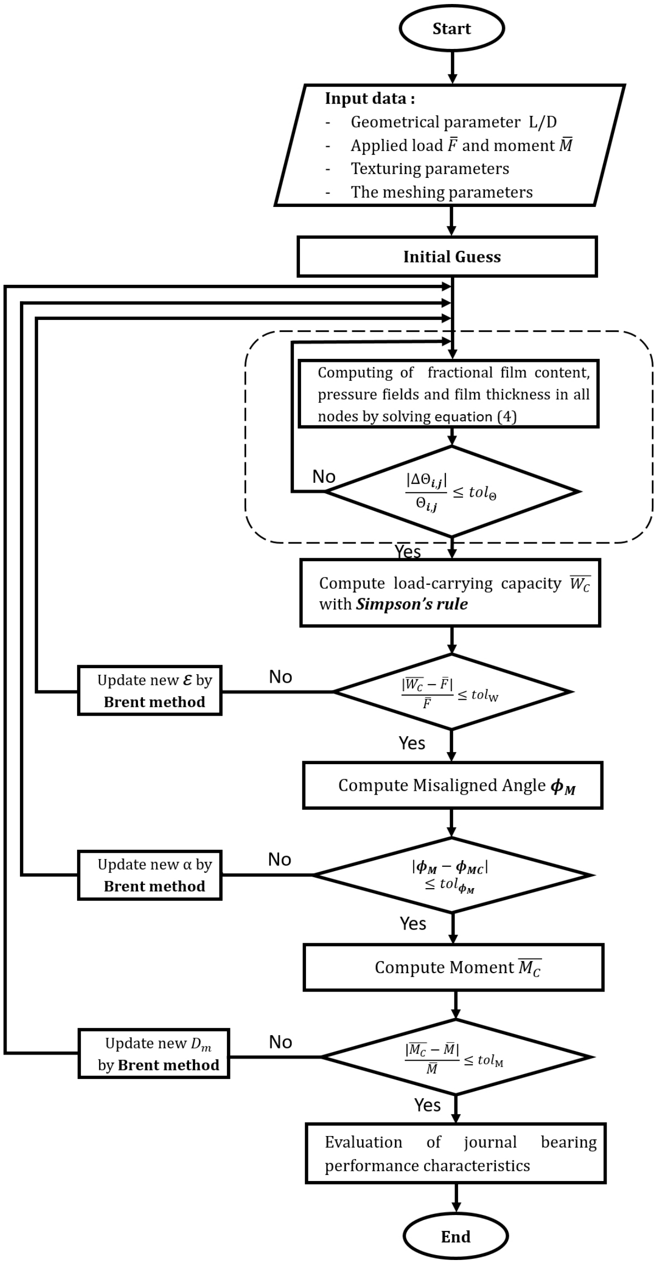

Figure 4: Flowchart of global computational procedure

2.5 Miscellaneous parameters

Performance characteristics of misaligned journal bearing for smooth/textured cases are computed using the following relations:

The dimensionless load components in the circumferential and the axial direction are given as:

$$\begin{cases} \overline{W}_\theta = & -\int_0^1 \int_0^{2\pi} \overline{P} \cos(\theta)\, d\theta\, dZ \\ \overline{W}_Z = & \int_0^1 \int_0^{2\pi} \overline{P} \sin(\theta)\, d\theta\, dZ \end{cases} \tag{15}$$

Then the total bearing load capacity and the attitude angle are:

$$\overline{W}_C = \sqrt{\overline{W}_\theta^2 + \overline{W}_Z^2}$$
$$\phi = \arctan\left(\frac{\overline{W}_\theta}{\overline{W}_Z}\right) \tag{16}$$

The dimensionless leakage flow-rate through the ends of the bearing, noted $\overline{Q}_1$ from the left-hand bearing end and $\overline{Q}_2$ from the right-hand bearing end, are given by:

$$\begin{cases} \overline{Q}_1 = -\int_0^1\int_0^{2\pi} \frac{1}{2}\frac{\partial \overline{P}}{\partial Z}\bar{h}^3\,\bar{y}\,(\bar{y}-1)\,d\theta d\bar{y} & for: Z=0 \\ \overline{Q}_2 = \int_0^1\int_0^{2\pi} \frac{1}{2}\frac{\partial \overline{P}}{\partial Z}\bar{h}^3\,\bar{y}\,(\bar{y}-1)\,d\theta d\bar{y} & for: Z=1 \end{cases} \tag{17}$$

then the total end lubricant flow rate is

$$\overline{Q}_Z = \left|\overline{Q}_1\right| + \left|\overline{Q}_2\right| \tag{18}$$

The dimensionless friction force acting on the journal surface is given by:

$$\overline{F}_t = \int_0^1\int_0^{\theta_S} \frac{1}{2}\frac{\partial \overline{P}}{\partial \theta}\bar{h}\,d\theta\,dZ + \int_0^1\int_0^{\theta_S} \frac{1}{\bar{h}}\,d\theta\,dZ + \int_0^1\int_{\theta_S}^{2\pi} \frac{\bar{h}_s}{\bar{h}^2}\,d\theta dZ \tag{19}$$

where, θ_s is the angular coordinate at the starting cavitation zone and $\bar{h}_s$ is the equivalent of oil film thickness in cavitation zone.

Consequently, the frictional coefficient is obtained as follows:

$$f\left(\frac{R}{C}\right) = \frac{\overline{F}_t}{\overline{W}} \tag{20}$$

Under misalignment, the bearing pressure is not symmetric to its mid-plane and it will produce some misaligned moments to act on the journal. Two dimensionless components of the moment, circumferential and axial can be written as follows:

$$\begin{cases} \overline{M}_\theta = \int_0^1\int_0^{2\pi} \overline{P}\,(Z-0.5)\,\sin\theta\,d\theta\,dZ \\ \overline{M}_Z = \int_0^1\int_0^{2\pi} \overline{P}\,(Z-0.5)\,\cos\theta\,d\theta\,dZ \end{cases} \tag{21}$$

then the total misalignment moment and its direction angle are:

$$\overline{M} = \sqrt{\overline{M}_\theta^2 + \overline{M}_Z^2} \tag{22}$$

$$\phi_M = \arctan\left(-\frac{\overline{M}_\theta}{\overline{M}_Z}\right) \tag{23}$$

All numerical integrations was carried-out by means of : SIMPSON rule.

3 Numerical results and discussions

3.1 Preliminary validation

Based on the analysis described in the present paper, a MATLAB computer program was developed. This section is devoted to the validation of our computational code. To this end, a comparison analysis is performed between the results of the present analysis and those from researchers works [22, 23, 52] for aligned/misaligned journal bearings with smooth/textured surfaces.

Case 1 : Misaligned journal bearing with smooth surface

1. Comparison with experimental results

   BOUYER and FILLON [22] performed experimental measurements in a misaligned journal bearing, and showed the maximum pressure in the mid-plane and the minimum film thickness, as a function of misaligned moment at a fixed bearing load. Figure 5 shows the comparison between the present predicted results, and those carried out by BOUYER and FILLON [22]. As the bearing is aligned, the moment is nil. When the moment increases, the maximum pressure and the minimum film thickness decreases. The results of the present comparison are in good agreement with those of the already mentioned paper [22]. It should be emphasized that the predicted results are slightly higher than those measured experimentally. The noticed differences are most probably due to the adopted assumptions : the negligibly cavitation pressure, Newtonian fluid in isothermal regime ($T = 40^{\circ}C$).

   The two dimensional results of film thickness, fractional-film content and pressure distributions obtained by the computational code are plotted in figure 6 and 7, for aligned (case $M = 0N.m$) and misaligned (case $M = 50N.m$) journal bearings, respectively, in order to further check its validity. In figure 6, the film thickness evolution remains constant in the axial direction, and, its minimum value occurs near $\theta = 181^{\circ}$. In fractional-film content distribution, the area where $\Theta \geq 1$ represents the full film region, and the area where $\Theta \leq 1$ represents the cavitation region; the variation in fractional film content in full film region is very small due to the large bulk modulus, while, in the cavitation region, drops significantly to $\Theta = 0.4$. However, a small variation in fractional film content in the full film region causes large change in the pressure distribution, as a results of the large value of the compressibility. Due to the atmospheric pressure imposed on the axial boundary, the fractional-film content at $z = 0$ and $z = L$ is assumed to be $\Theta = 1$, while on circumferential boundary, is due to the bearing oil supply conditions. The simulations also show the pressure distribution for aligned bearing, where, the maximum pressure occurs near $\theta = 138^{\circ}$ in the bearing mid-plane $z = L/2$.

   The influence of misalignment is shown very clearly in figure 7. The minimum film thickness occurs near $\theta = 140^{\circ}$ on the rear end $z = 0$ and near $\theta = 265^{\circ}$ on the front end $z = L$. The variation in the fractional film content in the axial direction is very severe, and, the cavitation region begins after the minimum film thickness and disappears in the bearing groove. Moreover, the boundary between the full film and the rupture regions is twisted severely, as a results of variation in axial minimum film thickness locations. The maximum pressure location is shifted to the rear end $z = 0$, and, its value is greater, compared to the aligned bearing. The highest pressure at each axial location occurs before the minimum film thickness, and its direction is roughly matching with the direction of the minimum film thickness.

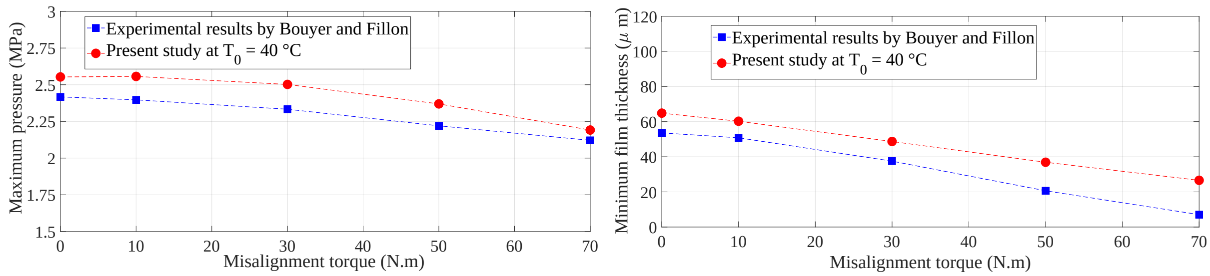

Input data:	$F = 9000\,(N)$	$N = 4000\,(rpm)$	$p_a = 0.08\,(MPa)$	$\mu = 0.0293\,(Pa.s)$	$T_0 = 40\,°C$	$\phi_M = 0°$
	$L = 80\,(mm)$	$D = 99.78\,(mm)$	$C = 117.5\,(\mu m)$	$l_G = 70\,(mm)$	$\psi_G = 0°$	$\Delta\psi_G = 18°$

Figure 5: Comparison present study with BOUYER and FILLON's experiments [22]

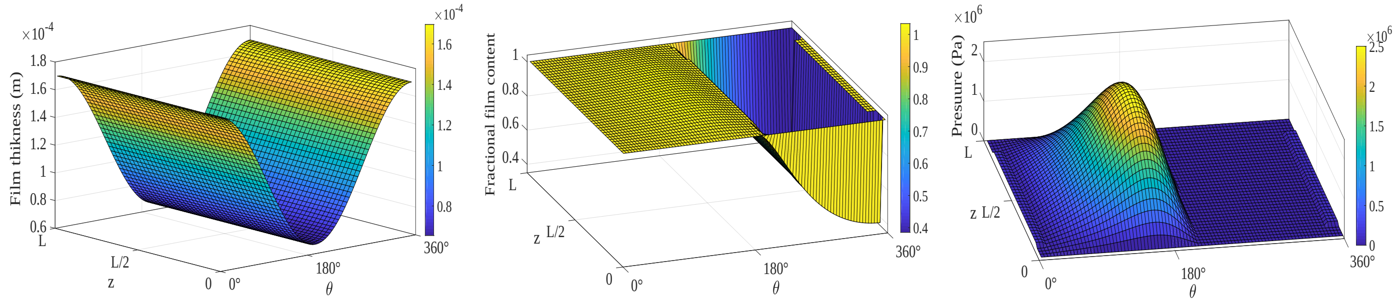

Figure 6: Film thickness evolution, fractional-film content and pressure distributions on the contact in an aligned journal bearing (case $M = 0\,N.m$)

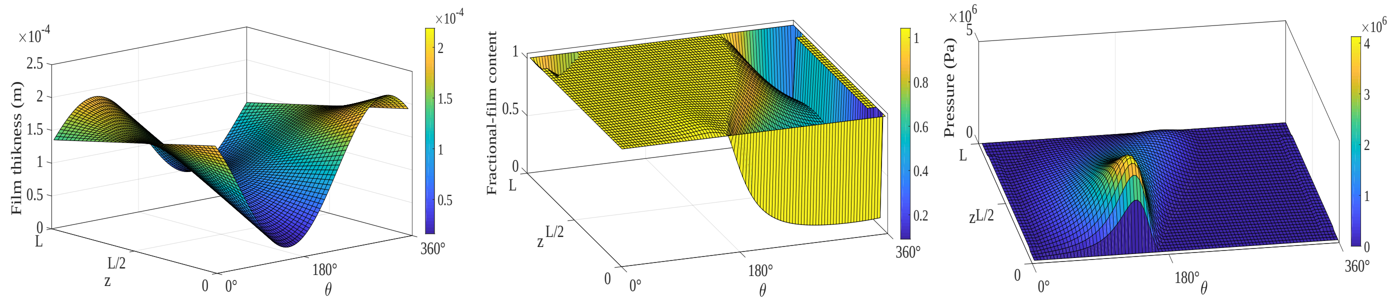

Figure 7: Film thickness evolution, fractional-film content and pressure distributions on the contact in misaligned journal bearing (case $M = 50\,N.m$)

2. Comparison with numerical results

Here, a comparison analysis is performed between our results and those computed by JANG and KHONSARI [23], for aligned/misaligned journal bearings with smooth surfaces.

Parameters adopted for this comparison are :

- Bearing data : (a) amplitude of external load $F = 20000\,N$; (b) amplitude of applied moment $M = 0\,\text{or}\,76\,N.m$; (c) applied moment diraction $\phi_M = 224.5°$; (d) journal diameter $D = 0.040\,m$; (e) bearing length $L = 0.080\,m$; (f) radial clearance $C = 0.00003\,m$; (j) rotational speed $N = 2500\,rpm$; (h) lubricant viscosity $\mu = 0.02\,Pa\,s$; (i) bulk modulus $\beta = 5\,GPa$.

- Computational method parameters : (a) finite-difference method (FDM) with JFO boundary conditions (b) grid size $(91, 41)$; (c) convergence criteria $tol_{\Theta} = 10^{-6}$, $tol_W = 10^{-4}$, $tol_M = 10^{-3}$, $tol_{\phi_M} = 10^{-2}$.

Table 2 presents the comparison between our predictions and those of the already mentioned paper [23]. It can be noted that the obtained values are very close to the reference ones with slight difference which may be due to the computational errors in the simulation.

Table 2: Comparison of performance characteristics of aligned/misaligned journal bearings

		Present study		JANG and KHONSARI [23]	
Imposed misalignment torque	$M\,(N.m)$	0	76	0	76
Eccentricity ratio	ε	0.395	0.373	0.392	0.378
Degree of misalignment	D_m	–	0.500	–	0.53
Angle on misalignment	α	–	121°	–	–
Maximum pressure	$P_{max}\,(MPa)$	5.799	6.976	5.90	6.81
Leakage flow-rate	$Q\,(cm^3/s)$	3.153	3.702	2.9	3.1
Attitude angle	ϕ^o	67.618	65.616	69.1	68.0
Friction coefficient	f	0.0037	0.0039	0.0039	0.0040

Case 2 : Textured journal bearing

In order to develop more confidence in the developed computer program, a comparison analysis is performed between our results and those of TALA-IGHIL et al. [52], for textured journal bearings with cylindrical dimple shape.

- Parameters adopted for this case are :
  - Bearing data : (a) amplitude of external load $F = 12\,600\,N$; (b) journal diameter $D = 0.063\,m$; (c) bearing length $L = 0.063\,m$; (d) radial clearance $C = 0.00003\,m$; (e) angular speed $\omega_1 = 625.4\,rad/s$; (f) lubricant viscosity $\mu = 0.0035\,Pa\,s$.
  - Bearing texture data : (a) cylindrical texture shape (b) texture radius $r_x = r_z = 1\,mm$; (c) texture depth $r_y = 0.015\,mm$.
  - Computational parameters : number of nodes per texture along : circumferential $nN_{t\,\theta} = 10$ and axial $nN_{t\,Z} = 10$ directions.
  - Computational method parameters : (a) finite-difference method (FDM) with Reynolds boundary conditions (b) grid size $(891, 142)$; (c) convergence criteria $tol_p = 10^{-4}$ and $tol_W = 10^{-5}$.

Unlike in TALA-IGHIL et al. [52] work, Simpson's rule was used to compute all numerical integrations and the Brent method [73] for the estimation of the new eccentricity ratio ε in the convergence loop.

The comparison results are presented in table 3. The results of the present comparison are in good agreement with one slight difference, which is due to the choice made concerning the numerical integration method.

In order to further show the effectiveness of our computational code, figures 8 and 9 present the prediction results for the film thickness and the pressure profile for smooth, fully and partially textured cases. The results present in these figures show very clearly the influence of textures on film thickness evolution and pressure profile, when compared to smooth surface bearing case.

Table 3: Comparison of performance characteristics of smooth/textured aligned journal bearings

		Present study			TALA-IGHIL et al. [52]		
		–	Fully	Partially	–	Fully	Partially
		Smooth	Textured		Smooth	Textured	
Eccentricity ratio	ε	0.6010	0.6995	0.5992	0.601	0.709	0.595
Minimum film thickness	$h_{min}\,(\mu m)$	11.969	9.0145	12.0245	11.97	8.71	12.16
Maximum pressure	$P_{max}\,(MPa)$	7.673	8.191	7.591	7.71	8.26	7.58
Attitude angle	ϕ^o	50.380	46.151	49.05	50.5	46.1	49.3
Axial flow	$Q\,\mathrm{x}\,10^{-5}\,(m^3/s)$	1.723	1.412	1.714	1.743	1.422	1.733

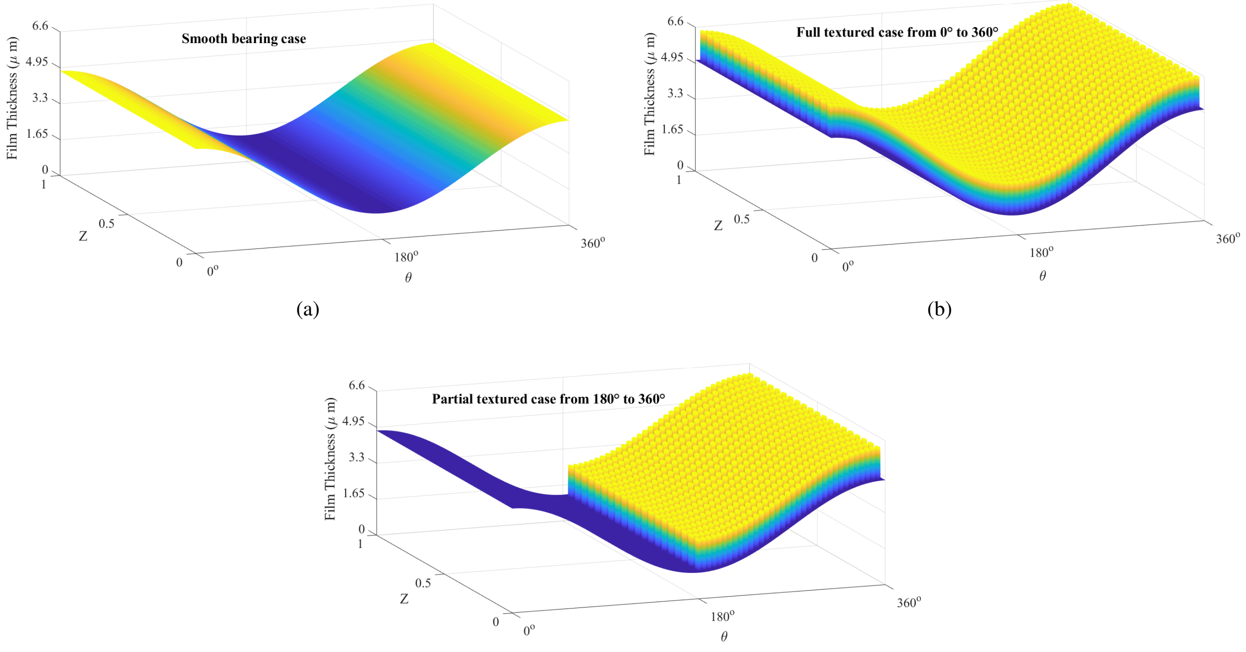

(a)

(b)

(c)

Figure 8: Film thickness evolution on the contact for smooth/textured journal bearings

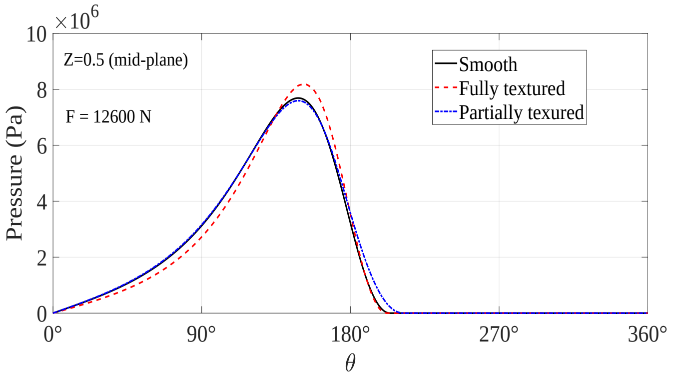

Figure 9: Pressure profile on the contact along the circumferential direction at bearing mid-plane for smooth/textured journal bearing cases

3.2 Performance analysis of textured misaligned journal bearing

In this section, our objective is to point out the preponderant effect (in terms of tribological properties) between bearing texture surface and journal misalignment. To achieve this end, a series of obtained results for smooth/textured bearing cases are presented to investigate the effect of the misalignment degree and angle on the performances of fully and partially textured journal bearings through three texture shapes (square “SQ”, cylindrical “CY” and triangular “TR”).

Bearing geometrical characteristics, as well as texturing parameters are given in table 4.

Table 4: Geometrical and Texturing parameters for the studied journal bearing

Geometrical parameters			Dimensionless variables	
Shaft diameter	$D\ (mm)$	40		
Bearing length	$L\ (mm)$	40	L/D	1
Radial clearance	$C\ (\mu m)$	50		
Eccentricity ratio	$e\ (\mu m)$	30	e/C	0.6
Texturing parameters				
Texture diameter	$d_x(mm)$	6	$\overline{d}_x = d_x/R$	0.3
Texture length	$d_z(mm)$	6	$\overline{d}_z = d_z/L$	0.15
Texture depth	$r_y\ (\mu m)$	25	$\overline{r}_y = r_y/C$	0.5
Texture number along the circumference	nC_θ	Full textured 16	Partial textured 8	
Texture number along the length	nC_z		5	
Operating conditions				
Journal speed	$N\ (rpm)$	3000		
Viscosity	$\mu\ (Pa\,s)$	0.05		
Bulk modulus	$\beta\ (MPa)$	100	40	
Grid size and convergence criteria				
Nodes per texture along the circumference	nN_{tx}		15	
Nodes per texture along the length	nN_{tz}		13	
Nodes in circumferential direction	nN_θ		421	
Nodes in axial direction	nN_z		121	
Nodes across the fluid film	nN_y		121	
Convergence criteria	tol_Θ		10^{-8}	

Figures 10 and 11 show the 3D representations of textured bearings. Note that, the bearing is with a line groove of negligible thickness, situated at the maximum film thickness and extending at the bearing ends.

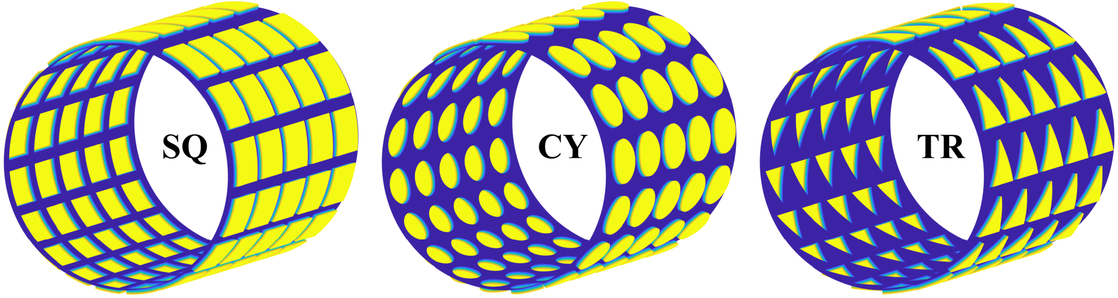

Figure 10: Geometrical representation of full textured bearing “0° to 360°” (square (left), cylinder (middle) and triangle (right))

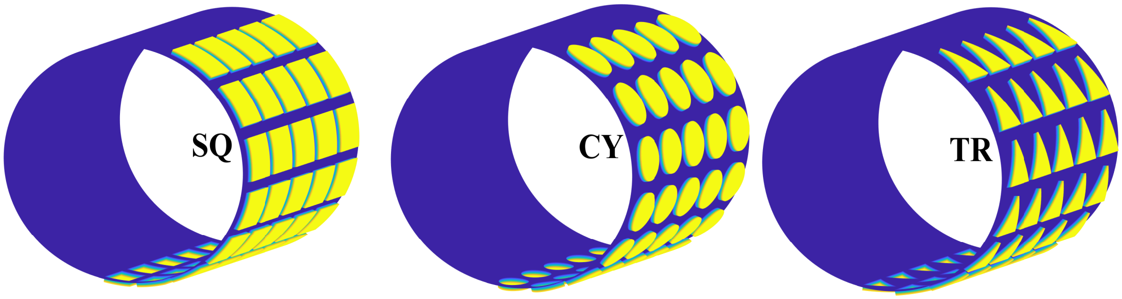

Figure 11: Geometrical representation of partial textured bearing “180° to 360°” (square (left), cylinder (middle) and triangle (right))

3.2.1 Textured aligned/misaligned journal bearing: 2D Versus 3D simulations

In order to examine the validity of three-dimensional 3D and two-dimensional 2D analysis of developed computational code, we provide benchmark results for smooth and full/partial textured aligned $(D_m = 0)$ and misaligned $(D_m = 0.75)$ journal bearings.

Figures 12, 13, 14 and 15 show the three-dimensional 3D distribution of lubricant film thickness computed at the contact interface for smooth, fully and partially textured bearings with square texture shape. In figure 12, the bearing is aligned, the film thickness evolution for smooth (figure 12a), fully textured (figure 12b) and partially textured (figure 12c) surface bearings remain constant in the axial direction, and, its minimum value occurs near $\theta = 181^\circ$. As the bearing is misaligned, the film thickness evolution for smooth (figure 13), fully textured (figure 14) and partially textured (figure 15) surface bearings, is plotted for three values of misalignment angle: (a) $\alpha = 0^\circ$, (b) $\alpha = 90^\circ$ and (c) $\alpha = 180^\circ$. Compared to aligned bearing, the minimum film thickness value occurs near $\theta = 181^\circ$, on the rear end $(z = 0)$ for $\alpha = 0^\circ$ (figures 13a, 14a and 15a), and on the front end $(z = L)$ for $\alpha = 180^\circ$ (figures 13b, 14b and 15b). While, in the case when $\alpha = 90^\circ$, the minimum film thickness occurs two values, near $\theta = 140^\circ$ on the rear end and near $\theta = 230^\circ$ on the front end (figures 13c, 14c and 15c).

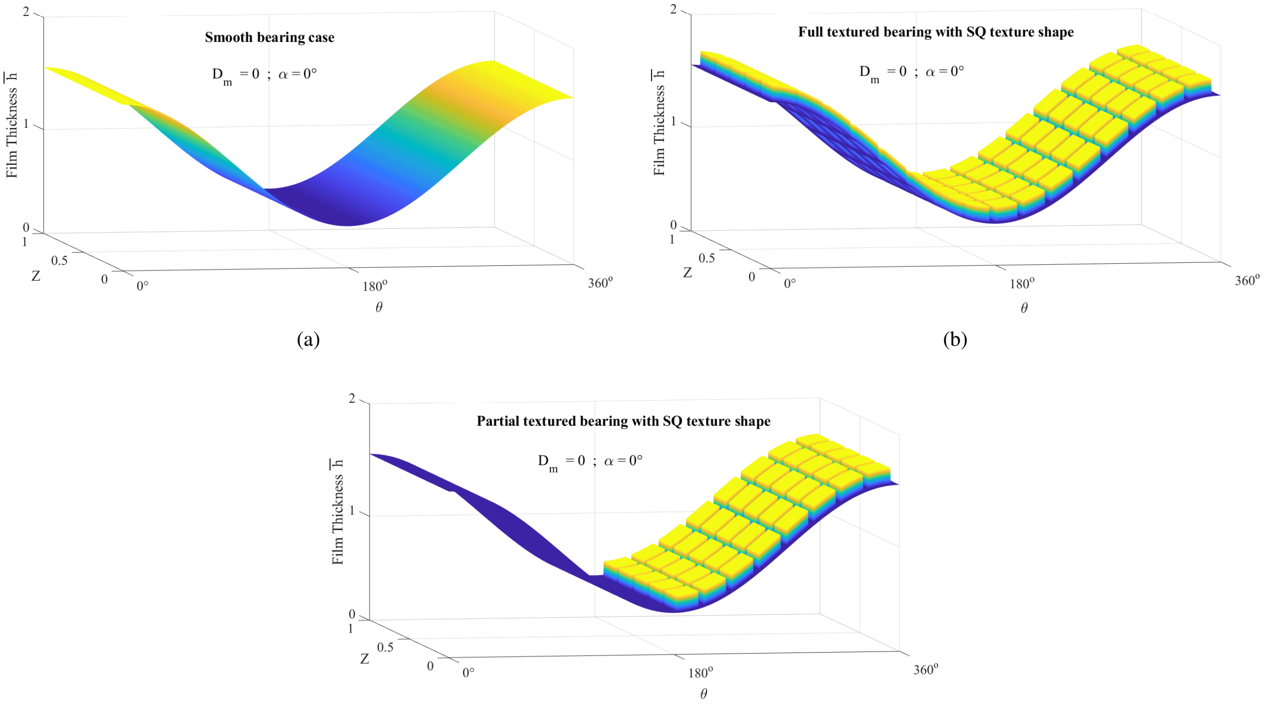

(a) (b) (c)

Figure 12: Evolution of dimensionless film thickness versus axial and circumferential coordinates for aligned journal bearing: (a) smooth bearing; (b) fully textured bearing (from 0° to 360°); (c) partially textured bearing (from 180° to 360°)

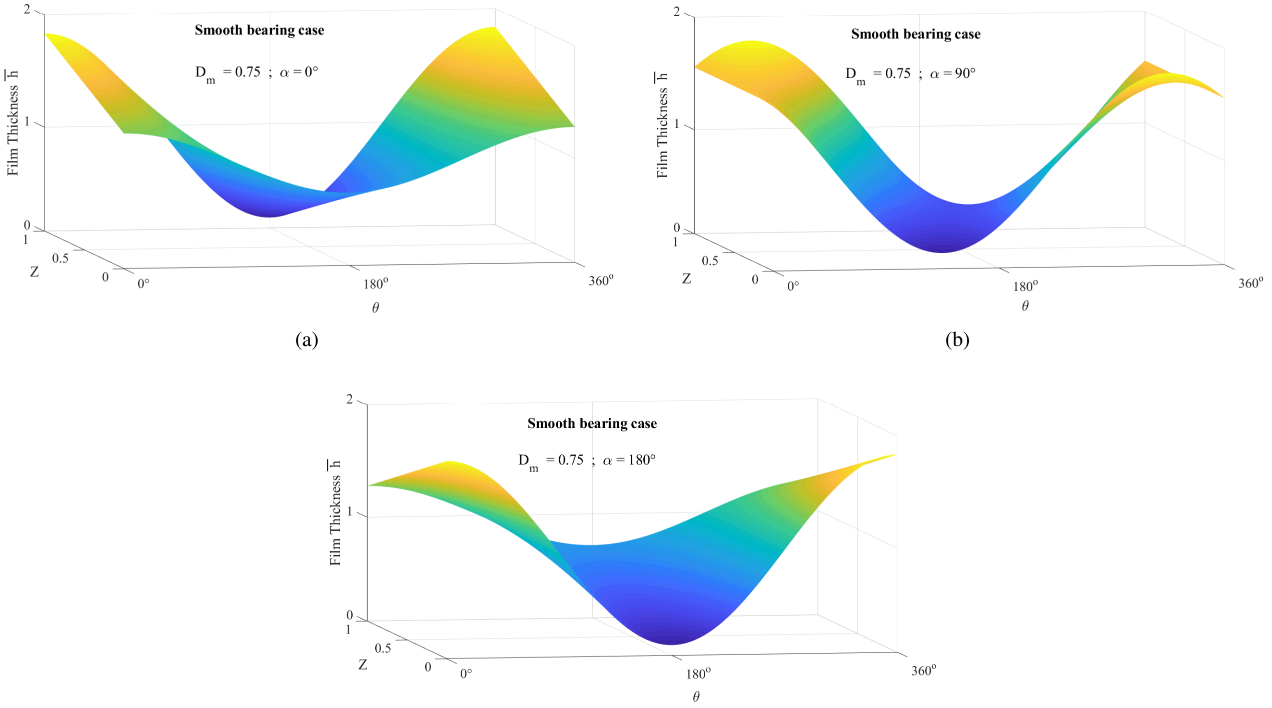

(a) (b) (c)

Figure 13: Evolution of smooth dimensionless film thickness versus axial and circumferential coordinates for misaligned journal bearing: (a) $\alpha = 0°$; (b) $\alpha = 90°$; (c) $\alpha = 180°$

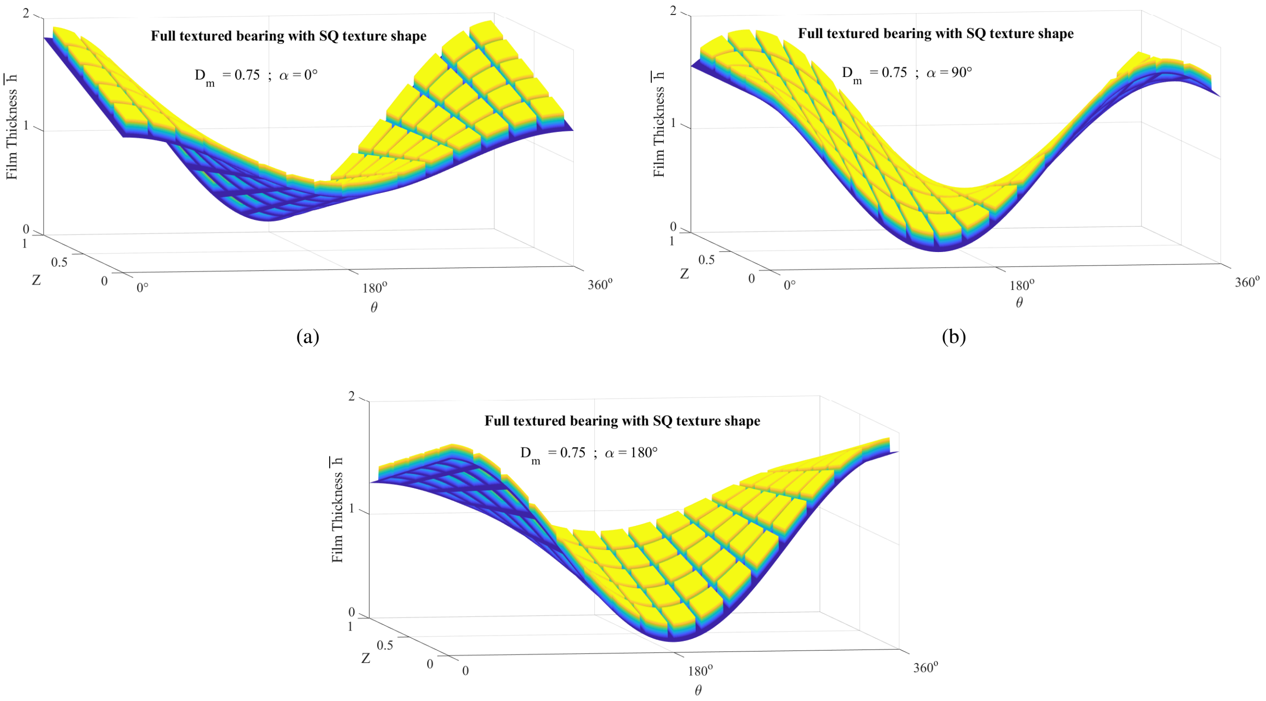

(a) (b) (c)

Figure 14: Evolution of fully textured dimensionless film thickness versus axial and circumferential coordinates for misaligned journal bearing: (a) $\alpha = 0°$; (b) $\alpha = 90°$; (c) $\alpha = 180°$

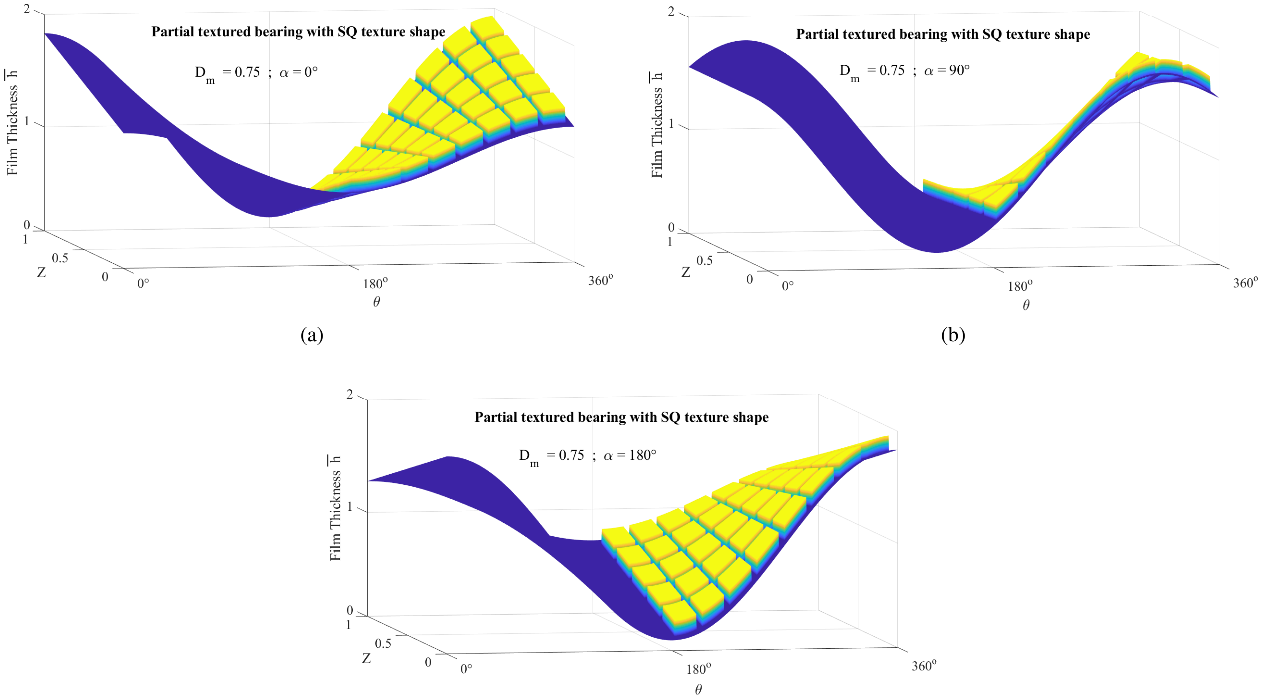

(a) (b) (c)

Figure 15: Evolution of partially textured dimensionless film thickness versus axial and circumferential coordinates for misaligned journal bearing: (a) $\alpha = 0°$; (b) $\alpha = 90°$; (c) $\alpha = 180°$

The variation in the dimensionless pressure distribution for smooth/textured surface aligned/misaligned journal bearings are shown in figures 16, 17, 18 and 19. As the bearing is aligned (figure 16), in smooth bearing case (figure 16a), the dimensionless maximum pressure location occurs near $\theta = 147.66°$ in the bearing mid-plane $z = L/2$, with the value of 2.95, which corresponds to $3.71\,MPa$, while, the maximum rupture angle reaches $\theta_{smax} = 189.80°$. Compared with the smooth bearing, in fully textured case (figure 16b), the angular position of $\overline{P}_{max}$ moves backward near $\theta = 137.90°$, and, its value decreases with about $56\,\%$, while, the maximum rupture angle value increases by $6.12°$. For partially textured case (figure 16c), the maximum pressure angular position moves forward near $\theta = 150.20°$, and, its value increases with about $5\,\%$, whereas, θ_{smax} increases by $12.25°$. Not that, when the rupture angle value increases, the full film region increases and then the cavitation area reduced, which causes in generation of additional hydrodynamic pressure and enhances the load lifting capacity. In the presence of misalignment ($D_m = 0.75$), the pressure distribution is plotted at various angles of misalignment (figure 17, 18 and 19), from these figures, is very clearly that the misalignment influenced the pressure fields in the axial direction and the location of the pressure peak. Compared to aligned journal bearing, for smooth bearing (figure 17), the maximum pressure location is shifted to the rear end for $\alpha = 0°$ (figure 17a) and to the front end for $\alpha = 180°$ (figure 17c), with a single peak appears at same circumferential location $\theta = 147.66°$, with the same value about 6.13, which corresponds to $7.70\,MPa$, twice larger than aligned bearing, while, the maximum rupture angle location remains constant $\theta_{smax} = 189.80°$ for both cases. For $\alpha = 90°$ (figure 17b) the maximum pressure occurs two values, near $\theta = 120°$ on the rear end and near $\theta = 190°$ on the front end, as a results of the two minimums of film thickness caused by this misalignment condition (figure 13c), the maximum rapture angle, also, shifted to the rear end near $\theta_{smax} = 227.75°$. Compared with the misaligned smooth bearing, in fully textured cases (figure 18), for $\alpha = 0°$ and $\alpha = 180°$, the location of $\overline{P}_{max}$ moves backward near $\theta = 144°$, and, its value decreases with about $59\,\%$, while, the maximum rupture angle value increases by $9.8°$. For $\alpha = 90°$, the maximum pressure location moves backward and the maximum rupture angle value increases with about $2\,\%$. For partially textured bearing cases (figure 19), the pressure peak location moves forward near $\theta = 150.10°$, for $\alpha = 0°$ and $\alpha = 180°$, and, its value increases with about $4.8\,\%$, while, θ_{smax} increases by $12.14°$. Furthermore, for $\alpha = 90°$, the maximum pressure location moves forward, while, the maximum rupture angle value decreases with 0.5%.

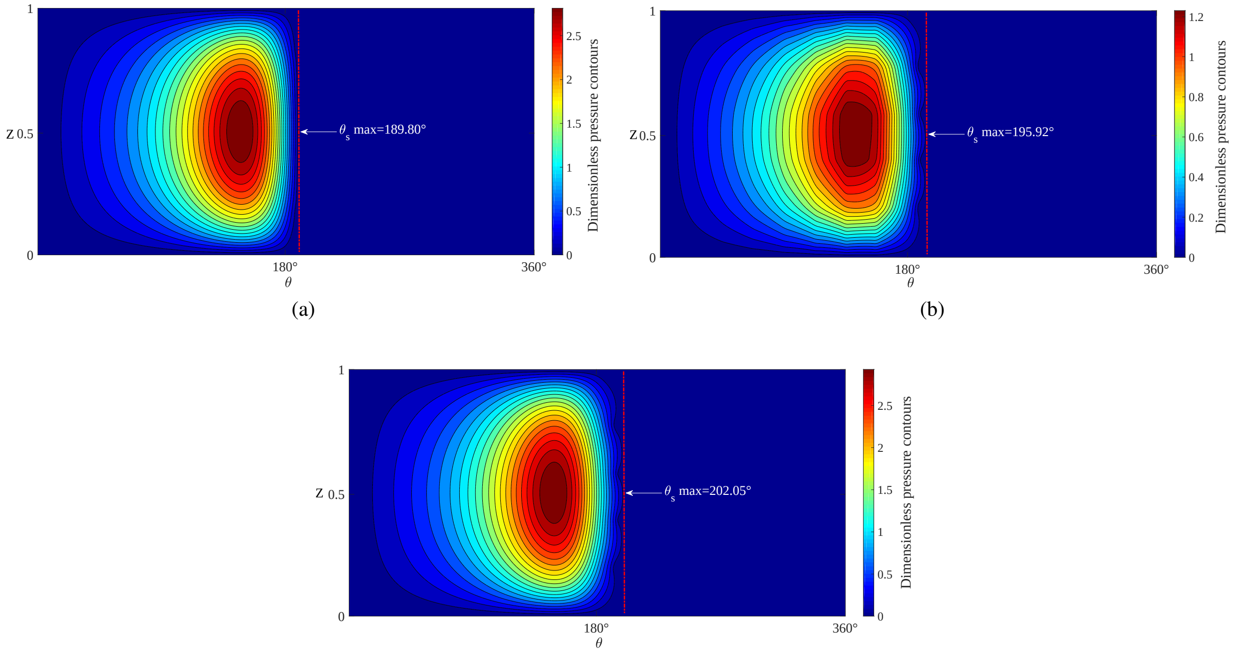

(a)

(b)

(c)

Figure 16: Distribution of dimensionless pressure versus axial and circumferential coordinates for aligned journal bearing: (a) smooth bearing; (b) fully textured bearing (from 0° to 360°); (c) partially textured bearing (from 180° to 360°)

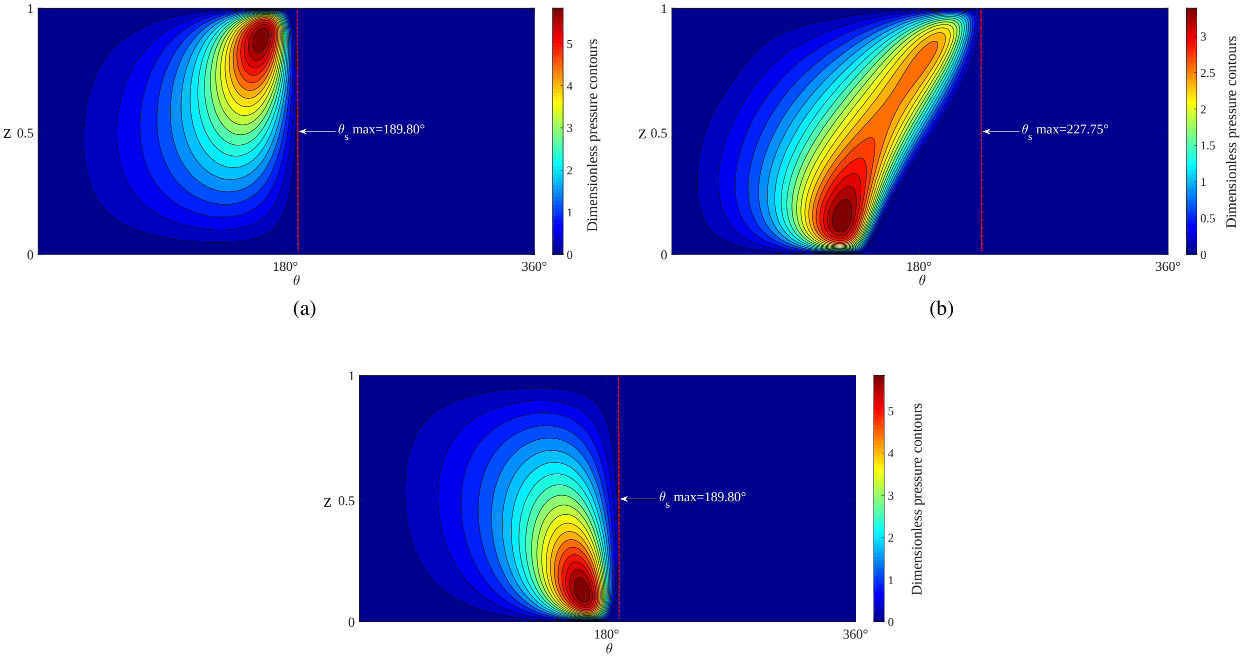

(a) (b) (c)

Figure 17: Distribution of smooth dimensionless pressure versus axial and circumferential coordinates for misaligned journal bearing: (a) $\alpha = 0°$; (b) $\alpha = 90°$; (c) $\alpha = 180°$

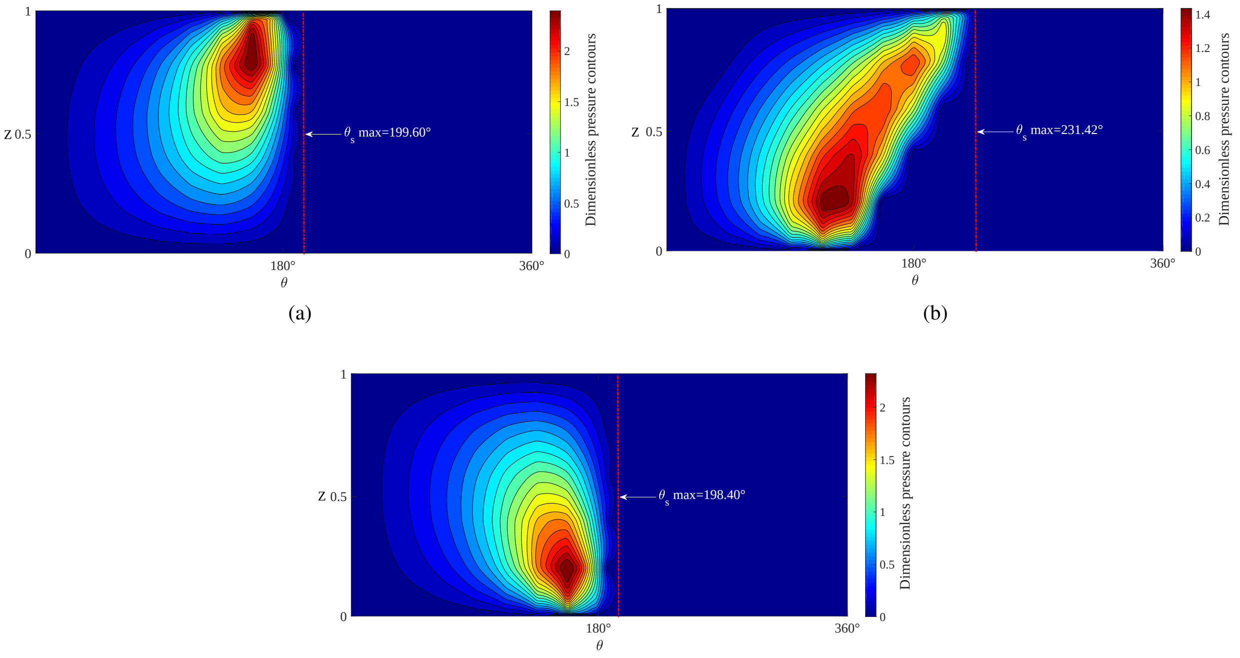

(a) (b) (c)

Figure 18: Distribution of fully textured dimensionless pressure versus axial and circumferential coordinates for misaligned journal bearing: (a) $\alpha = 0°$; (b) $\alpha = 90°$; (c) $\alpha = 180°$

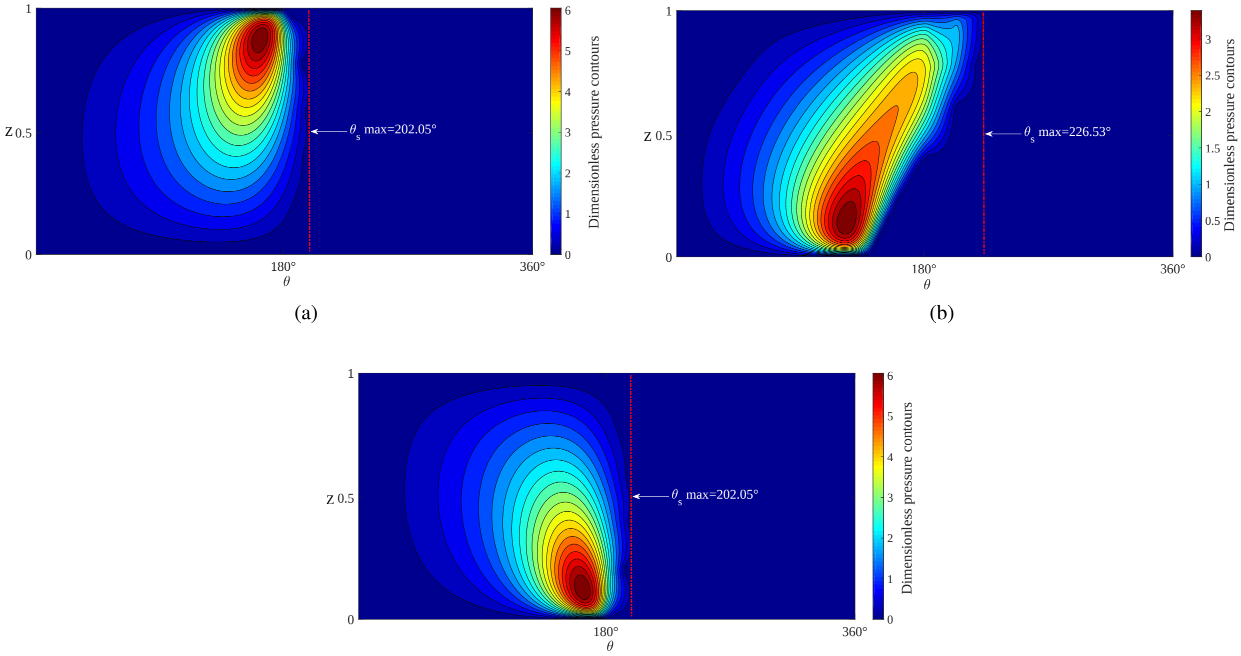

(a) (b)

(c)

Figure 19: Distribution of partially textured dimensionless pressure versus axial and circumferential coordinates for misaligned journal bearing: (a) $\alpha = 0°$; (b) $\alpha = 90°$; (c) $\alpha = 180°$

The effect of texture shapes on two-dimensional 2D pressure profile for aligned/misaligned journal bearings is visualized in figures 20, 21 and 22. Each figure is plotted in circumferential direction, at the mid-plane for aligned bearings and in rear end $(Z = 0.15)$, front end $(Z = 0.75)$ and mid-plane $(Z = 0.5)$ for misaligned bearings. In the absence of misalignment, in fully textured cases (figure 20a), the dimensionless film pressure for all considered texture shapes are less than the smooth case. This can be explained by the fact that, dimple shapes with flat bottoms ("SQ", "CY" and "TR") have a micro-step bearing mechanism. Due to this mechanism, the micro-step bearing causes a much large film thickness divergence, so a significant pressure drop (in full-film region) and a smaller pressure recovery will be generated (in rupture film region). As the texture contour geometry increases, the micro-pressure drop effect increases. Unlike the previous case, a significant improvement on pressure profile caused by partially textured features is clearly shown in figure 20b, as a results of micro-pressure recovery mechanism, which causes a nil pressure drop in full-film region and a highest pressure recovery will be generated in rupture film region. For misaligned bearings, Fully textured features (figure 21) reduce the pressure profile at any section, while, partially textured features increase the pressure profile (figure 22), as a results of micro-step bearing mechanism.

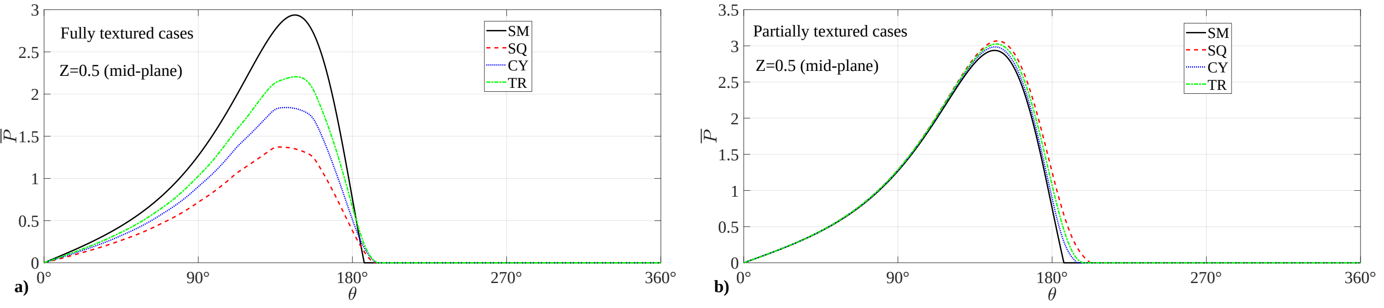

(a) (b)

Figure 20: Effect of texture shapes on two-dimensional pressure distribution along the circumferential direction at bearing mid-plane for aligned journal bearing: (a) fully textured cases (from 0° to 360°) ; (b) partially textured cases (from 180° to 360°)

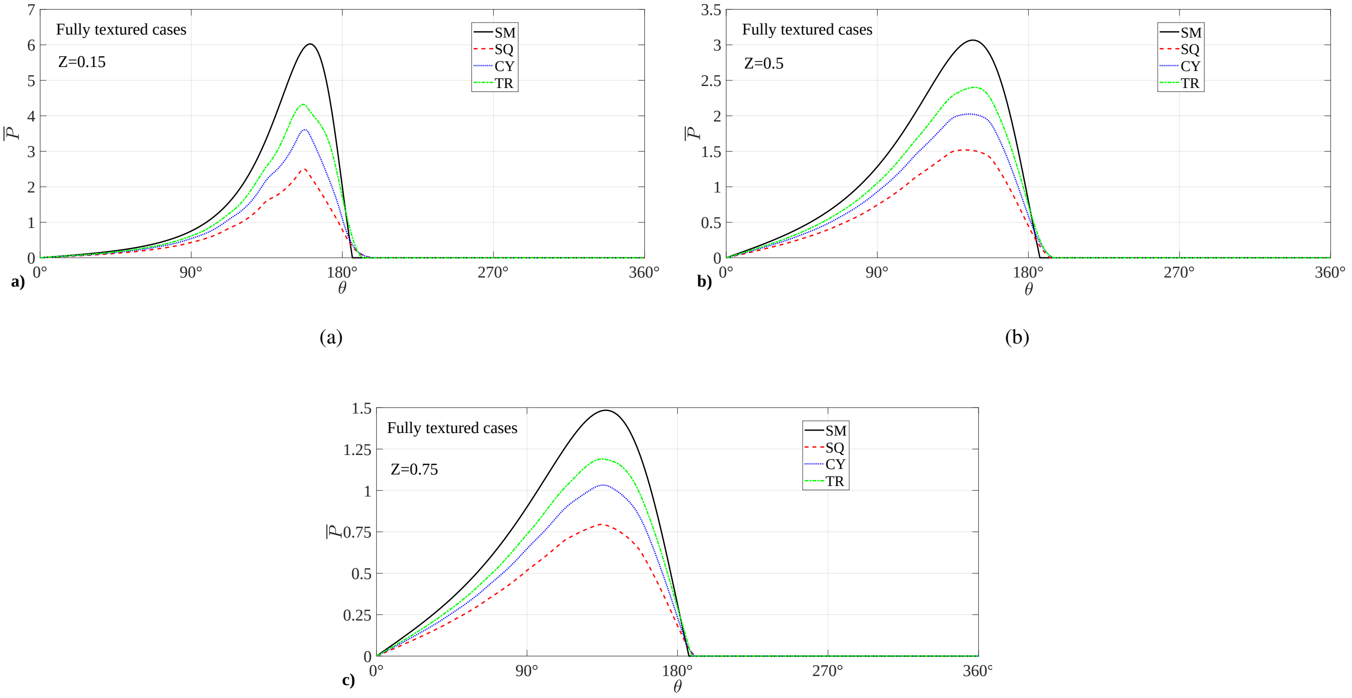

(a)

(b)

(c)

Figure 21: Effect of fully texture shapes on two dimensional pressure distribution along the circumferential direction at: (a) $Z = 0.15$; (b) $Z = 0.5$; (c) $Z = 0.75$ for misaligned journal bearing ($D_m = 0.75$, $\alpha = 180^{\circ}$)

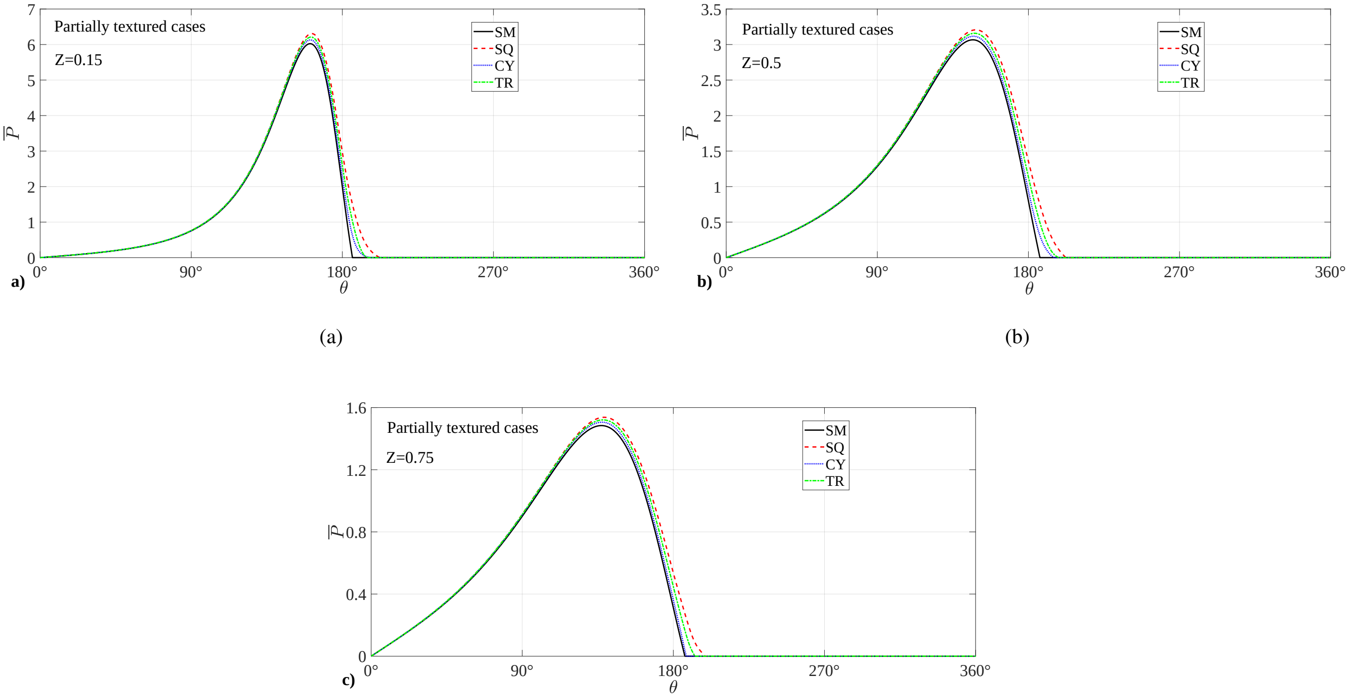

(a)

(b)

(c)

Figure 22: Effect of partially texture shapes on two dimensional pressure distribution along the circumferential direction at: (a) $Z = 0.15$; (b) $Z = 0.5$; (c) $Z = 0.75$ for misaligned journal bearing ($D_m = 0.75$, $\alpha = 180^{\circ}$)

In the next subsections, the obtained results for smooth/textured misaligned bearing cases are compared in terms of : maximum pressure, leakage flow-rate, load-carrying capacity, load-attitude angle, friction force and coefficient, misalignment moment and moment direction.

3.2.2 Influence of degree of misalignment D_m

The curves of a number of bearing performance parameters as a function of the degree of misalignment are shown in figures 23a – 23h (for smooth and full/partial textured bearing surface cases). Note that in this subsection, the misalignment angle α is fixed at $\alpha = 180°$, while the degree of misalignment varies in the range of $(0 - 0.9)$.

The curves of dimensionless maximum pressure $\overline{P}_{max}$ for various degree of misalignment D_m; is shown in figure 23a. It is found that the rate of increase in $\overline{P}_{max}$ for all considered cases is pronounced at higher values of misalignment degree D_m (especially when $D_m > 0.5$), simply due to the smaller minimum film thickness. It should be emphasized that, when $D_m = 0$ the bearing is aligned, and when $D_m \to 1$, the minimum film thickness $\overline{h}_{min} \to 0$ (surfaces come into direct contact), and the maximum pressure $\overline{P}_{max} \to \infty$. Moreover, previous figure also show the comparative graph for smooth, fully and partially textured bearing surfaces. Maximum pressure values are clearly different from those recorded for the smooth surface. In addition, it can be seen from this figure that the main feature of fully texturing bearing surfaces is to reduce the maximum pressure, as a results of micro-pressure drop effect. While, partially texturing gradually increase the maximum pressure, this behavior is due to the dimple pressure recovery generated by textures in the rupture film region.

In figure 23b, the leakage flow-rate $\overline{Q}_Z$ slightly increases with increasing degree of misalignment, which can be justified by the large pressure gradient on the both ends. It is also visible that, in the case of fully textured bearings, all considered texture shapes reduce the leakage flow-rate, which is in fact resulting from the larger pressure drop by the presence of dimples in full film bearing surface. While, in the case of partially textured bearings, all considered dimples increase slightly the leakage flow-rate, which is due to the fact that pressure field trend to accumulate inside the texture cavity (micro-pressure recovery mechanisms) and thus adding a supplementary pressure which increase the pressure gradient.

Figure 23c shows that, the load-carrying capacity increases with increasing degree of misalignment. Firstly, the increase in $\overline{W}_C$ has the same behavior as the previous dimensionless maximum pressure (figure 23a) for smooth and full/partial textured cases. Secondly, texturing the whole bearing surface does not enhance the load carrying capacity, while partial texturing causes a significant improvement in $\overline{W}_C$. These results can be justified by the presence of flat bottom profiles micro-step bearing mechanism (explained previously), which causes, in full film region, a thicker film thickness, and so largest pressure drop (presenting a bad performance in $\overline{W}_C$). While, in rupture film region, a significant pressure recovery will be generated (presenting an improvement in $\overline{W}_C$), these results are consistent with those described in [64]. Here, an emphasis is placed on the texture contour geometry, which present a key parameter in flat bottom profile contour geometry. In fully texturing case, as the texture contour geometries increases, the micro-step bearing mechanism effects increases (highest film thickness divergence and largest pressure drop). In partially texturing case, square texture shape performed the best hydrodynamic enhancement, followed by the triangle and circlr, which confirms the results obtained by ZHANG et al. [69].

Beside the load-carrying capacity, the figure 23d presents the variation of the load-attitude angle ϕ against the degree of misalignment D_m for smooth/textured surface bearings. It can be discerned from the figure that for any studied texture shapes for full/partial textured cases, the values of load-attitude angle are obviously different from those of smooth surfaces. However, ϕ decreases with the increase in D_m, this decrease is more considerable at higher values of degree of misalignment to support the large bearing load. For fully texturing features, the load attitude angle increases compared to the smooth surface bearing case, as a results of decreases load, while the main features of partially texturing is to increase the load attitude angle compared to the smooth surface case, which is due to the increases of bearing load.

The evolution of dimensionless friction force F_t and friction coefficient $f \, . \, (R/C)$ for different values of degree of misalignment D_M in cases of smooth/textured surface bearings are shown in figures 23e and 23f, respectively. In figure 23e, it is noticed that for all considered configurations (smooth and full/partial textured surface bearing), the friction force increases with the increase of D_m, and it is also visible that all texture feature reduce the friction force. However, compared to the friction force (figure 23e), the resulting friction coefficients values have an opposite trend. Moreover, it can be also observed that, the friction coefficient $f.(R/C)$ decreases with the increases of degree of misalignment D_M, for all studied cases. However, in the case of fully textured bearings, the friction coefficients increases compared to the smooth surface case, presenting a bad performance. This is due to the fact that the flat bottom profiles causes a pressure drop, which decreases the load carrying capacity, and so increases the friction values. In the other case of partially textured bearings, the square shape "SQ" shows the greatest friction reduction, followed by the triangle and circle. This is due to the increase in load carrying capacity, caused by the pressure recovery of these textures.

The total misalignment moment M and its direction angle ϕ_M are computed at the given misalignment conditions and plotted in figures 23g and 23h, respectively. It can be noticed that, both bearing moment and its direction angle increase with increasing degree of misalignment, This is due to the larger pressure and its asymmetric shape. Furthermore, texturing the whole bearing surface reduces the bearing moment and the moment angle for any texture shapes, compared to the smooth surface, as a results of micro-pressure drop mechanisms. While, partially surface texturing increases the misalignment moment and its direction angle, presenting a good performance, which also results from textures micro-pressure recovery mechanism.

3.2.3 Influence of misalignment angle α

The bearing performance parameters at various angle of misalignment are presented in table 5. Note that in this subsection, the degree of misalignment D_m is fixed at $D_m = 0.75$, while the angle of misalignment varies in the range of $(0° - 180°)$. Moreover, the case where the misalignment angle varies from $180° \rightarrow 360°$ is not presented in the table since both cases are physically the same, observed in an opposite direction (i.e. at $\alpha = 0°$ the results is the same as those at $\alpha = 180°$).

From table 5, it can be seen that the computed dimensionless maximum pressure and dimensionless leakage flow-rate of smooth/textured journal bearings decreases till the position $\alpha = 90°$ and then increases with increasing α. This behavior can be explained by the fact that, the minimum film thickness increases with increasing α until $\alpha = 90°$ and then decreases with increasing α. The other noticeable points in table 5 are the decrease in the maximum pressure and leakage flow-rate after the incorporating of textures in full bearing surface, which explained previously by micro-pressure drop effect. Moreover, the increase in the maximum pressure and leakage flow-rate when the second half of bearing surface is textured, is a results of micro-pressure recovery mechanism.

The variation of the dimensionless bearing load is similar to that of the dimensionless maximum pressure. As mentioned above, the produced pressure in partially textured surface bearing enhances the load lifting capacity, and so decreases the load attitude angle values and friction coefficient. While the fully textured cases cause a net load loss, and so increases the load attitude angle values and the friction coefficient. Table 5, also presents the variation of dimensionless friction force, it can be noticed that, corresponding to each misalignment angle α, all textures reduce the computed friction force values. Moreover, it is worth noting that, when α approaches to 0° or 180°, the misalignment moment and its direction increases, this can be justified by the fact that, the maximum pressure occurs near the front or rear end. For any misalignment angle α, as the whole bearing surface is textured, the moment and its direction decreases, while the partially textured bearing surfaces improve the misalignment moment and its direction.

3.2.4 Influence of eccentricity ratio ε

In the previous subsections, the effect of journal misalignment in smooth/textured bearing surfaces is studied by varying the misalignment angle (α from 0° to 180°) and degree (D_m from 0 to 0.9), while, the eccentricity ratio ε was set to $\varepsilon = 0.6$. Here, various eccentricity ratios (ε from 0.5 to 0.9), fixed misalignment angle ($\alpha = 180°$) and degree ($D_m = 0.75$) are considered. Computed performance characteristics as a function of eccentricity ratios are plotted in figure 24a–24h. The results observed is that: as the eccentricity ratio increases, the dimensionless bearing performances such as: maximum pressure, leakage flow-rate, bearing load, friction force and the moment increase due to the decrease in the minimum film thickness, while the load attitude angle and friction coefficient decrease due to the large bearing load. Fully textured bearings have a detrimental effects (reducing the load-carrying capacity, misalignment moment, and increasing the friction coefficient). While partially textured bearings perform better by increasing the load lifting capacity, misalignment moment and lowering the friction coefficient and is more pronounced at higher values of eccentricity ratios ε. This is clearly due to the micro-step bearing effect, which can positively or negatively affects the tribological characteristics of the misaligned journal bearing (much depends to texture zone location).

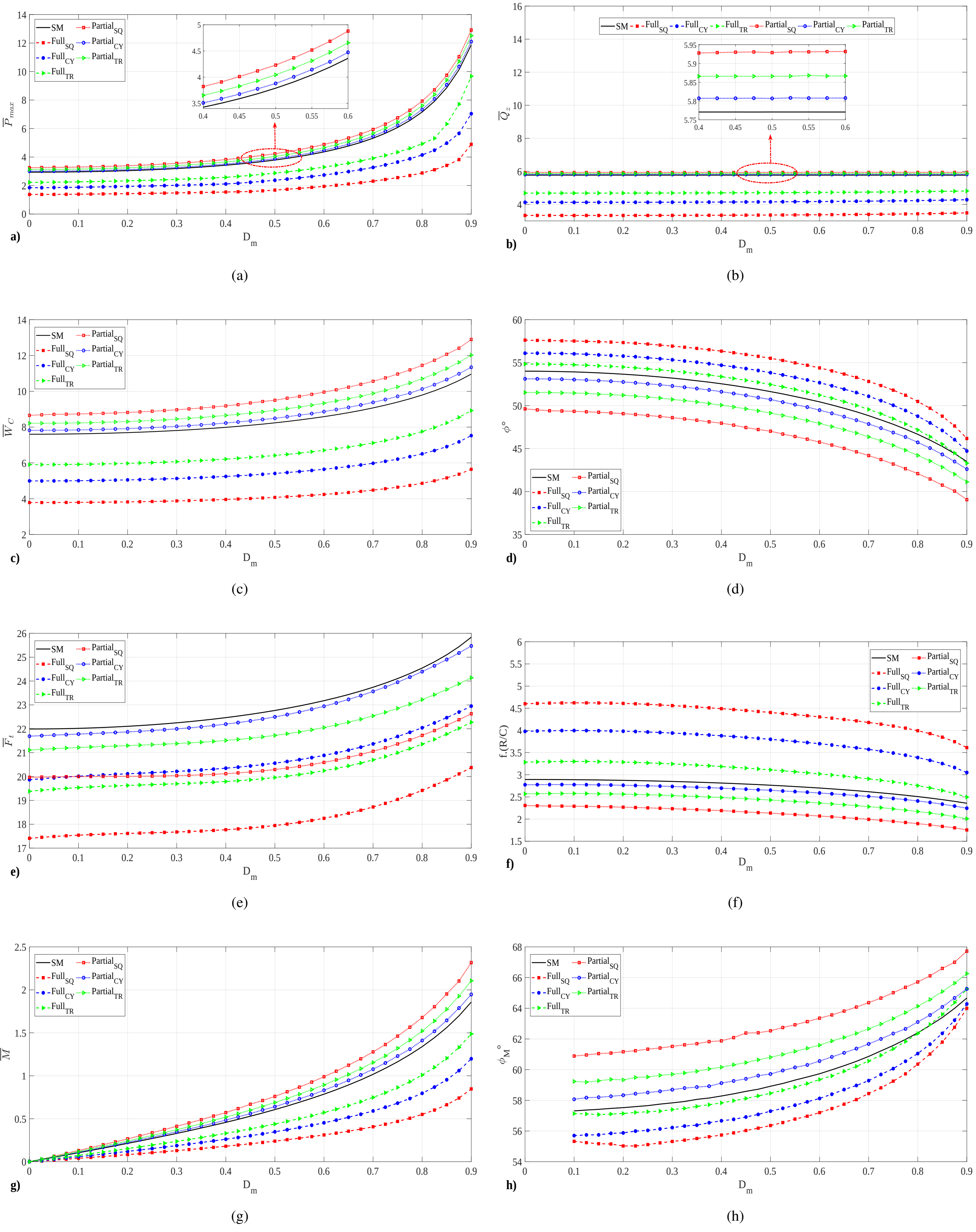

(a) (b) (c) (d) (e) (f) (g) (h)

Figure 23: Variation in bearing performances with degree of misalignment for smooth/textured surface bearings for: $\Lambda = 1$; $\varepsilon = 0.6$; $\alpha = 180°$

Table 5: Variation in dimensionless bearing performances with angle of misalignment for smooth/textured surface bearing for: $\Lambda = 1$; $\varepsilon = 0.6$; $D_m = 0.75$

α			0°	30°	60°	90°	120°	150°	180°		0°	30°	60°	90°	120°	150°	180°
Full textured	SM	Maximum pressure	6,072	5,584	4,414	3,514	5,212	5,998	6,075	Leakage flow-rate	5,771	5,580	5,296	4,913	5,155	5,554	5,771
	SQ		2,638	2,362	1,887	1,551	2,220	2,426	2,554		3,479	3,336	3,157	2,988	3,073	3,287	3,412
	CY		3,701	3,312	2,684	2,151	3,138	3,536	3,647		4,257	4,090	3,869	3,678	3,801	4,057	4,213
	TR		4,388	4,046	3,266	2,616	3,680	4,370	4,345		4,786	4,605	4,366	4,098	4,287	4,576	4,757
Partial textured	SQ		6,710	6,108	4,638	3,516	5,223	6,040	6,751		5,927	5,620	5,305	4,989	5,183	5,603	5,934
	CY		6,236	5,734	4,564	3,515	5,218	6,017	6,229		5,808	5,604	5,300	4,956	5,173	5,563	5,809
	TR		6,460	5,982	4,636	3,515	5,220	6,025	6,463		5,870	5,610	5,304	4,962	5,174	5,578	5,870
Full textured	SM	Load-carrying capacity	9,391	9,060	8,354	8,102	8,840	9,345	9,396	Load-attitude angle	47,854	46,108	45,684	52,223	53,028	50,220	47,829
	SQ		4,774	4,605	4,141	4,077	4,440	4,615	4,645		51,064	48,863	49,812	53,308	55,996	54,118	51,802
	CY		6,310	6,116	5,521	5,424	5,941	6,185	6,211		49,635	47,223	47,911	52,949	54,516	52,419	50,042
	TR		7,459	7,104	6,460	6,354	6,935	7,244	7,395		48,302	46,956	46,996	52,322	54,0176	51,669	48,488
Partial textured	SQ		10,857	9,968	8,396	8,195	8,909	9,656	10,965		43,529	42,939	44,985	50,956	52,828	49,212	43,201
	CY		9,723	9,395	8,363	8,161	8,853	9,493	9,718		46,863	45,065	45,489	51,482	53,009	49,743	46,867
	TR		10,230	9,631	8,374	8,163	8,894	9,506	10,249		45,441	44,024	45,078	51,034	52,869	49,744	45,377
Full textured	SM	Friction force	24,104	47,574	45,346	39,266	29,986	27,950	24,104	Friction coefficient	2,5667	5,251	5,428	4,846	3,392	2,991	2,565
	SQ		19,064	29,943	28,458	24,859	19,998	18,473	18,954		3,993	6,503	6,871	6,097	4,504	4,003	4,081
	CY		20,943	34,945	33,334	29,236	22,924	21,329	21,468		3,319	5,714	6,038	5,390	3,859	3,448	3,456
	TR		20,998	39,470	37,141	32,574	25,214	23,576	20,932		2,815	5,556	5,749	5,126	3,636	3,255	2,830
Partial textured	SQ		21,502	31,911	31,539	29,007	24,592	23,288	21,380		1,980	3,201	3,766	3,540	2,760	2,412	1,950
	CY		23,893	40,246	38,458	34,453	27,318	25,449	23,911		2,457	3,822	4,2682	3,945	2,942	2,602	2,460
	TR		22,936	36,808	35,696	32,204	26,167	24,703	22,824		2,242	4,284	4,580	4,221	3,086	2,677	2,227
Full textured	SM	Misalignment moment	1,162	1,114	0,953	0,864	0,946	1,114	1,163	Misalignment direction	61,552	73,583	87,901	30,887	28,530	48,851	61,575
	SQ		0,517	0,525	0,428	0,390	0,389	0,443	0,469		59,953	73,130	89,531	36,868	23,886	44,682	59,249
	CY		0,720	0,729	0,592	0,539	0,567	0,651	0,681		60,460	73,498	89,875	33,939	26,577	46,444	60,066
	TR		0,888	0,850	0,715	0,644	0,695	0,790	0,864		61,458	73,076	89,131	32,684	27,504	46,882	61,361
Partial textured	SQ		1,437	1,380	1,033	0,958	0,957	1,120	1,462		64,717	75,841	88,738	32,009	29,387	49,826	65,016
	CY		1,232	1,316	1,007	0,918	0,953	1,118	1,230		62,364	74,083	88,324	31,382	29,103	49,670	62,354
	TR		1,317	1,180	1,018	0,928	0,957	1,115	1,320		63,276	75,329	88,617	31,779	29,329	49,743	63,332

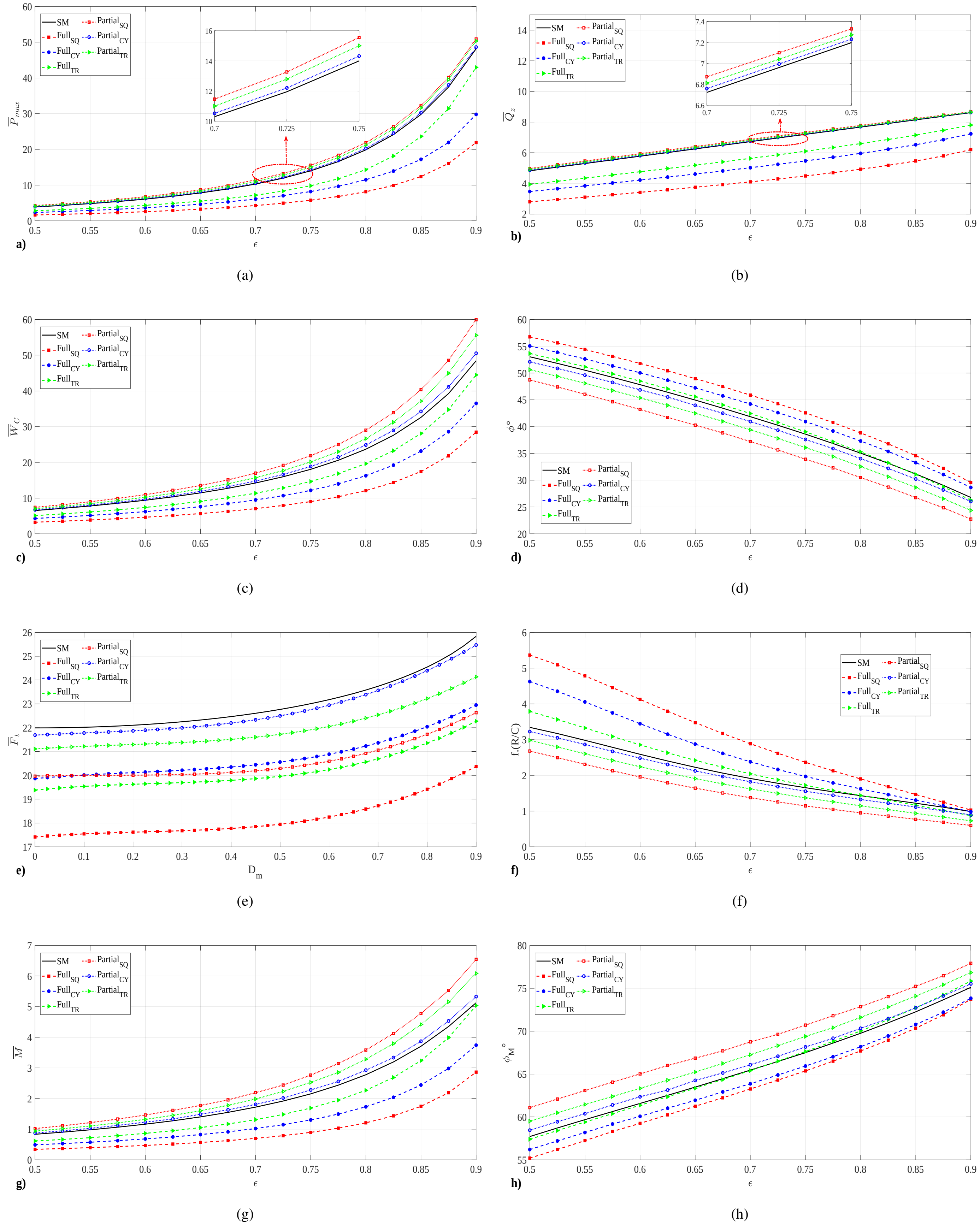

(a) (b)

(c) (d)

(e) (f)

(g) (h)

Figure 24: Bearing performances versus eccentricity ratio for smooth/textured surface bearings for: $\Lambda = 1$; $D_m = 0.75$; $\alpha = 180°$

4 Conclusion

In this paper, a numerical study was conducted to highlight the potential of combined influences of bearing surface texturing and journal misalignment on the performance characteristics of hydrodynamic journal bearings. Three texture shapes with flat bottoms: square (SQ), cylindrical (CY) and triangular (TR) and shaft misalignment variation in angle α , and degree D_m, were considered. The model employed herein was solved by means of finite difference technique with taking into account the lubrication film rupture and reformation by adopting the mass-conserving cavitation algorithm ("JFO" boundary conditions). The predictions made with the present numerical model were validated against available theoretical and experimental data in the literature.

The findings from the present numerical investigation can be summarized in the following points:

1. The texture contour geometry and its location has proved to be key parameters in journal bearing performances.
2. Fully textured bearing with flat/constant bottom dimples poorly affect the main bearing performances as compared to the smooth case, which is directed by micro-pressure drop effect, Moreover, as the texture contour geometry increases, the micro-pressure drop effect increases. While, partially texturing significantly enhance all bearing performances, which can be explained by the effect of micro-pressure recovery mechanism. These facts were more noticeable at high eccentricity ratios, high misalignment degrees and when α approaches to 0° or 180°.
3. The square "SQ" texture shape appears to be the most favorable to improve the misaligned bearing performances, followed by the triangular "TR" then cylindrical "CY".
4. As the degree of misalignment increases, the maximum pressure, the leakage flow-rate, the bearing load, the friction force and the moment increase due to the decrease in the minimum film thickness, while the load attitude angle and friction coefficient decrease due to the large bearing load. Also the inclusion of textures at requisite location can compensate the reduces bearing performances caused by shaft misalignment, especially when $\alpha \to 0^\circ$ or $\alpha \to 180^\circ$.
5. The previous observations concerning texturing the second angular part of the bearing (beyond 180°), are due to the micro-pressure recovery effect, which generates additional hydrodynamic pressure and serve as fluid reservoirs that provides lubricant to the contact in starvation cases, and so, enhance the main bearing performances.
6. The optimum textured location depends strongly on the geometrical parameters (type of misalignment) and the operating conditions of the journal bearings.

The conducted study is constrained by the selected texturing parameters; fixed density, number, disposition, orientation and dimension; the chosen problem assumptions; by applying Newtonian rheology and mass-conserving cavitation; selected geometrical parameters: bearing length and diameter, eccentricity ratio and misalignment condition, and neglecting changes in viscosity, density and temperature, etc. On one hand, breaking these constraints will open to us new possibilities of finding the optimum texture shapes required to each bearing configuration, on the other hand, difficulties on the computational aspect will be faced (CPU-time and cost). The need of efficient and fast algorithms becomes more than necessary. In this context, considerable efforts have been made by our research team to efficiently reduce the computation time using model order reduction (MOR) [74]. The application of this technique for the simulation of textured misaligned journal bearing is planned as the next step of this research.

Appendix

e_0	Eccentricity at the bearing mid-plane(m)
e'	Magnitude of the projection of the misaligned journal axis on the mid-plane (m)
C	Radial clearance (m)
D	Bearing diameter (m)
D_m	Degree of misalignment
L	Bearing length (m)
R	Bearing radius (m)
F	External applied force (N)
g	Cavitation switching function
U	shaft speed ($^m/_s$)
x, y, z	Global Coordinate system (m)
r_x, r_z, r_y	Texture dimensions (m)
h	Film thickness (m)
Δh	Variation of film thickness due to the presence of the texture (m)
p	Lubricant pressure (Pa)
p_c	Cavitation pressure (Pa)
p_{max}	Maximum pressure (Pa)
W_C	Load-carrying capacity
Q_z	Leakage flow-rate(m^3/s)
F_t	Friction force ($N.m$)
$f\,.\,(^R/_C)$	Friction coefficient
M	Misalignment moment ($N.m$)
nC_θ, nC_z	Number of textures along circumferential θ and axial Z directions
tol_Θ	Relative convergence criterion on pressure
tol_W	Relative convergence criterion on load
tol_M	Relative convergence criterion on moment magnitude
tol_{ϕ_M}	Relative convergence criterion on moment direction
$\overline{P}_{max}$	Dimensionless maximum pressure
$\overline{W}_C$	Dimensionless load-carrying capacity
$\overline{Q_z}$	Dimensionless axial film flow

$\overline{F}_t$	Dimensionless friction force
$\overline{M}$	Dimensionless moment
$\overline{h}$	Dimensionless film thickness $[h/C]$
$\overline{h}_s$	Dimensionless equivalent of oil film thickness in cavitation zone
$\overline{\Delta h}$	Dimensionless variation of film thickness due to the presence of the texture
$\overline{P}$	Dimensionless lubricant pressure
$\overline{P_c}$	Dimensionless cavitation pressure
θ, $\bar{y}$, Z	Dimensionless global Coordinate system
$\overline{r_x}$, $\overline{r_z}$, $\overline{r_y}$	Dimensionless texture dimensions
α	Angle between ϕ_0 and the rear center of the misaligned journal
β	Bulk modulus (Pa)
$\overline{\beta}$	Dimensionless bulk modulus
ρ	Fluid density of the oil (kg/m^3)
ρ_c	Fluid density at the cavitation pressure (kg/m^3)
Θ	Fractional film content $\Theta = \rho/\rho_c$
Λ	Aspect ratio $\Lambda = L/D$
ϕ	Attitude angle (deg)
ϕ_M	Misalignment direction (deg)
ω	Angular velocity (rad/s)
μ	Dynamic viscosity $(Pa\,s)$
ε	Eccentricity ratio $\varepsilon = e_0/C$
ε'	Misalignment eccentricity ratio $\varepsilon' = e'/C$
θ_s	Angular position of the rupture zone (deg)

References

[1] Khonsari, Michael M and Booser, E Richard. *Applied tribology: bearing design and lubrication*, vol. 12. John Wiley & Sons, 2008. 1

[2] Mufti, RA and Priest, M. Theoretical and experimental evaluation of engine bearing performance. *Proceedings of the Institution of Mechanical Engineers, Part J: Journal of Engineering Tribology*, 223(4):629–644, 2009. 1

[3] Jang, Joon Young and Khonsari, Michael M. On the characteristics of misaligned journal bearings. *Lubricants*, 3(1):27–53, 2015. 1

[4] A, McKee. S. and R, McKee. T. Pressure distribution in oil films of journal bearings. *Tribology International*, 57:149–165, 1932. 1

[5] Dubois, GB, Mabie, Hamilton Horth, and Ocvirk, Fred W. Experimental investigation of oil film pressure distribution for misaligned plain bearings. NACA Technical Note 2507(3), 1951. 1

[6] DuBois, GB, Ocvirk, FW, and Wehe, RL. Properties of misaligned journal bearings. *Trans. ASME*, 79(1205-1):2, 1957. 1

[7] Smalley, AJ and McCallion, H. Paper 5: The effect of journal misalignment on the performance of a journal bearing under steady running conditions. in *Proceedings of the Institution of Mechanical Engineers, Conference Proceedings*, vol. 181, pp. 45–54. SAGE Publications Sage UK: London, England, 1966. 1

[8] Singh, DV, Sinhasan, R, and Pal, Roshan. Performance characteristics of an ungrooved big-end bearing with misalignment. *Tribology transactions*, 32(2):234–238, 1989. 1

[9] Stokley, JR and Donaldson, RR. Misalignment effects in 180° partial journal bearings. *ASLE TRANSACTIONS*, 12(3):216–226, 1969. 1

[10] Ausman, JS. Torque produced by misalignment of hydrodynamic gas-lubricated journal bearings. *Journal of Basic Engineering*, 82(2):335–340, 1960. 1

[11] Rice, John R. Misalignment torques of hydrodynamic gas-lubricated journal bearings. *Journal of Basic Engineering*, 87(1):193–198, 1965. 1

[12] Monmousseau, P and Fillon, M. Analysis of static and dynamic misaligned tilting-pad journal bearings. *Proceedings of the Institution of Mechanical Engineers, Part J: Journal of Engineering Tribology*, 213(4):253–261, 1999. 1

[13] El-Butch, AM and Ashour, NM. Transient analysis of misaligned elastic tilting-pad journal bearing. *Tribology international*, 38(1):41–48, 2005. 1

[14] San Andres, Luis. The effect of journal misalignment on the operation of a turbulent flow hydrostatic bearing. *Journal of tribology*, 115(3):355–363, 1993. 1

[15] Jain, Satish C, Sharma, Satish C, and Nagaraju, T. Misaligned journal effects in liquid hydrostatic non-recessed journal bearings. *Wear*, 210(1-2):67–75, 1997. 1

[16] Medwell, JO and Gethin, DT. Synthesis of thermal effects in misaligned hydrodynamic journal bearings. *International journal for numerical methods in fluids*, 6(7):445–458, 1986. 1

[17] Arumugam, P, Swarnamani, S, and Prabhu, BS. Effects of journal misalignment on the performance characteristics of three-lobe bearings. *Wear*, 206(1-2):122–129, 1997. 1

[18] Pinkus, Oscar and Bupara, SS. Analysis of misaligned grooved journal bearings. *Journal of Lubrication Technology*, 101(4):503–509, 1979. 1

[19] Ikeuchi, K.; Katsuse, S.; Hamamura K.; Mori H. Effects of misalignment in full journal bearing with circumferential oil groove. *Proceedings of the JSLE International Tribology Conference, Tokyo, Japan*, 101:67–72, 1985. 1

[20] D, Vijayaraghavan. and G., Keith. T. *Effect of cavitation on the performance of a grooved misaligned journal bearing*, vol. 134: 377 - 397. Wear, 1989. 1, 2.1, 1

[21] D, Vijayaraghavan. and G., Keith. T. *Analysis of a finite grooved misaligned journal bearing considering cavitation and starvation effects*, vol. 112: 60 - 67. ASME. J. Tribol, 1990. 1

[22] Bouyer, J and Fillon, M. Improvement of the thd performance of a misaligned plain journal bearing. *Journal of tribology*, 125(2):334–342, 2003. 1, 2.1, 3.1, 1, 5

[23] Jang, JY and Khonsari, MM. On the behavior of misaligned journal bearings based on mass-conservative thermohydrodynamic analysis. *Journal of Tribology*, 132(1):011702, 2010. 1, 2.1, 3.1, 2, **??**

[24] Kumar, Punit and Khonsari, MM. Traction in ehl line contacts using free-volume pressure-viscosity relationship with thermal and shear-thinning effects. *Journal of Tribology*, 131(1):011503, 2009. 1

[25] He, Zhen-peng, Zhang, Jun-hong, Xie, Wei-song, Li, Zhou-yu, and Zhang, Gui-chang. Misalignment analysis of journal bearing influenced by asymmetric deflection, based on a simple stepped shaft model. *Journal of Zhejiang University SCIENCE A*, 13(9):647–664, 2012. 1

[26] Elsharkawy, Abdallah A. Effects of misalignment on the performance of flexible porous journal bearings. *Tribology transactions*, 46(1):119–127, 2003. 1

[27] Gulwadi, Sanjay D and Shrimpling, Gary. Journal bearing analysis in engines using simulation techniques. tech. rep., SAE Technical Paper, 2003. 1

[28] Safar, ZS, Elkotb, MM, and Mokhtar, DM. Analysis of misaligned journal bearings operating in turbulent regime. *Journal of tribology*, 111(2):215–219, 1989. 1

[29] Xu, Guohui, Zhou, Jian, Geng, Haipeng, Lu, Mingjian, Yang, Lihua, and Yu, Lie. Research on the static and dynamic characteristics of misaligned journal bearing considering the turbulent and thermohydrodynamic effects. *Journal of Tribology*, 137(2):024504, 2015. 1

[30] Osman, Tarek Abdel. Misalignment effect on the static characteristics of magnetized journal bearing lubricated with ferrofluid. *Tribology Letters*, 11(3-4):195–203, 2001. 1

[31] Das, Santanu, Guha, SK, and Chattopadhyay, AK. On the steady-state performance of misaligned hydrodynamic journal bearings lubricated with micropolar fluids. *Tribology International*, 35(4):201–210, 2002. 1

[32] Zhang, Xiuli, Yin, Zhongwei, Jiang, Dan, Gao, Gengyuan, Wang, Yanzhen, and Wang, Xinbo. Load carrying capacity of misaligned hydrodynamic water-lubricated plain journal bearings with rigid bush materials. *Tribology International*, 99:1–13, 2016. 1

[33] Abdel-Latif, LA and Mokhtar, MOA. Misalignment effects on hydrodynamicaly lubricated journal bearings with rough surfaces. *Wear*, 128(3):225–237, 1988. 1

[34] Guha, SK. Analysis of steady-state characteristics of misaligned hydrodynamic journal bearings with isotropic roughness effect. *Tribology International*, 33(1):1–12, 2000. 1

[35] Sharma, Satish C, Jain, SC, and Nagaraju, T. Combined influence of journal misalignment and surface roughness on the performance of an orifice compensated non-recessed hybrid journal bearing. *Tribology transactions*, 45(4):457–463, 2002. 1

[36] Sun, Jun, Deng, Mei, Fu, Yonghong, and Gui, Changlin. Thermohydrodynamic lubrication analysis of misaligned plain journal bearing with rough surface. *Journal of Tribology*, 132(1):011704, 2010. 1

[37] Patir, Nadir and Cheng, HS. An average flow model for determining effects of three-dimensional roughness on partial hydrodynamic lubrication. *Journal of lubrication Technology*, 100(1):12–17, 1978. 1

[38] Patir, Nadir and Cheng, HS. Application of average flow model to lubrication between rough sliding surfaces. *Journal of Lubrication Technology*, 101(2):220–229, 1979. 1

[39] Qiu, Mingfeng, Minson, Bret R, and Raeymaekers, Bart. The effect of texture shape on the friction coefficient and stiffness of gas-lubricated parallel slider bearings. *Tribology International*, 67:278–288, 2013. 1

[40] Etsion, Izhak. State of the art in laser surface texturing. *Transactions of the ASME-F-Journal of Tribology*, 127(1):248, 2005. 1

[41] Wang, Xiaolei and Kato, Koji. Improving the anti-seizure ability of sic seal in water with rie texturing. *Tribology Letters*, 14(4):275–280, 2003. 1

[42] Stephens, Lyndon Scott, Siripuram, Ravi, Hayden, Matthew, and McCartt, Bianca. Deterministic micro asperities on bearings and seals using a modified liga process. in *ASME Turbo Expo 2002: Power for Land, Sea, and Air*, pp. 573–580. American Society of Mechanical Engineers, 2002. 1

[43] Schneider, Yu G. Formation of surfaces with uniform micropatterns on precision machine and instruments parts. *Precision engineering*, 6(4):219–225, 1984. 1

[44] Greco, Aaron, Raphaelson, Steven, Ehmann, Kornel, Wang, Q Jane, and Lin, Chih. Surface texturing of tribological interfaces using the vibromechanical texturing method. *Journal of manufacturing science and engineering*, 131(6):061005, 2009. 1

[45] Wakuda, Manabu, Yamauchi, Yukihiko, Kanzaki, Shuzo, and Yasuda, Yoshiteru. Effect of surface texturing on friction reduction between ceramic and steel materials under lubricated sliding contact. *Wear*, 254(3):356–363, 2003. 1

[46] Hamilton, DB, Walowit, JA, and Allen, CM. A theory of lubrication by micro-irregularities. *Journal of Basic Engineering*, 88(1):177–185, 1966. 1

[47] Wakuda, Manabu, Yamauchi, Yukihiko, Kanzaki, Shuzo, and Yasuda, Yoshiteru. Effect of surface texturing on friction reduction between ceramic and steel materials under lubricated sliding contact. *Wear*, 254(3):356–363, 2003. 1

[48] Varenberg, M, Halperin, G, and Etsion, I. Different aspects of the role of wear debris in fretting wear. *Wear*, 252(11):902–910, 2002. 1

[49] Yamakiri, Hiroki, Sasaki, Shinya, Kurita, Tsuneo, and Kasashima, Nagayoshi. Effects of laser surface texturing on friction behavior of silicon nitride under lubrication with water. *Tribology International*, 44(5):579–584, 2011. 1

[50] Lu, Xiaobin and Khonsari, MM. An experimental investigation of dimple effect on the stribeck curve of journal bearings. *Tribology Letters*, 27(2):169, 2007. 1

[51] Tala-Ighil, Nacer and Fillon, Michel. A numerical investigation of both thermal and texturing surface effects on the journal bearings static characteristics. *Tribology International*, 90:228–239, 2015. 1

[52] Tala-Ighil, Nacer, Fillon, Michel, and Maspeyrot, Patrick. Effect of textured area on the performances of a hydrodynamic journal bearing. *Tribology International*, 44(3):211–219, 2011. 1, 2.3, 3.1, 3.1, **??**

[53] Kango, S, Sharma, RK, and Pandey, RK. Thermal analysis of microtextured journal bearing using non-newtonian rheology of lubricant and jfo boundary conditions. *Tribology International*, 69:19–29, 2014. 1, 2.1

[54] Elrod, HG and Adams, MLt. A computer program for cavitation and starvation problems. *Cavitation and related phenomena in lubrication*, 103:37–41, 1974. 1, 2.1, 2.1

[55] Zhang, Hui, Dong, Guangneng, Hua, Meng, Guo, Feifei, and Chin, Kwai Sang. Parametric design of surface textures on journal bearing. *Industrial lubrication and Tribology*, 67(4):359–369, 2015. 1

[56] Anno, James N, Walowit, JA, and Allen, CM. Microasperity lubrication. *Journal of Lubrication Technology*, 90(2):351–355, 1968. 1

[57] Tønder, Kristian. Inlet roughness tribodevices: dynamic coefficients and leakage. *Tribology International*, 34(12):847–852, 2001. 1

[58] Tønder, K. Hydrodynamic effects of tailored inlet roughnesses: extended theory. *Tribology International*, 37(2):137–142, 2004. 1

[59] Etsion, Izhak and Burstein, L. A model for mechanical seals with regular microsurface structure. *Tribology Transactions*, 39(3):677–683, 1996. 1

[60] Olver, AV, Fowell, MT, Spikes, HA, and Pegg, IG. 'inlet suction', a load support mechanism in non-convergent, pocketed, hydrodynamic bearings. *Proceedings of the Institution of Mechanical Engineers, Part J: Journal of Engineering Tribology*, 220(2):105–108, 2006. 1

[61] Fowell, M, Olver, AV, Gosman, AD, Spikes, HA, and Pegg, I. Entrainment and inlet suction: two mechanisms of hydrodynamic lubrication in textured bearings. *Journal of Tribology*, 129(2):336–347, 2007. 1

[62] Yagi, Kazuyuki and Sugimura, Joichi. Balancing wedge action: a contribution of textured surface to hydrodynamic pressure generation. *Tribology Letters*, 50(3):349–364, 2013. 1

[63] Nanbu, Toshikazu, Ren, Ning, Yasuda, Yoshiteru, Zhu, Dong, and Wang, Q Jane. Micro-textures in concentrated conformal-contact lubrication: effects of texture bottom shape and surface relative motion. *Tribology Letters*, 29(3):241–252, 2008. 1

[64] Uddin, MS, Ibatan, Tom, and Shankar, S. Influence of surface texture shape, geometry and orientation on hydrodynamic lubrication performance of plane-to-plane slider surfaces. *Lubrication Science*, 29(3):153–181, 2017. 1, 3.2.2

[65] Jakobsson, Bengt. The finite journal bearing considering vaporization. *Trans. Chalmers Univ. of Tech, Sweden*, 190, 1965. 2.1

[66] Olsson, Karl-Olof. Cavitation in dynamically loaded bearing. *Trans. Chalmers Univ. of Tech, Sweden*, 308, 1957. 2.1

[67] Ausas, Roberto, Ragot, Patrick, Leiva, Jorge, Jai, Mohammed, Bayada, Guy, and Buscaglia, Gustavo C. The impact of the cavitation model in the analysis of microtextured lubricated journal bearings. *Journal of Tribology*, 129(4):868–875, 2007. 2.1, 2.4

[68] P, Maspeyrot and Frene, J. Paper iii (i) comparison between aligned and misaligned bearings under dynamic loading in both quasi-static and dynamic misalignment. *Tribology Series*, 18(7):19–26, 1991. 1

[69] Zhang, YL, Zhang, XG, and Matsoukas, G. Numerical study of surface texturing for improving tribological properties of ultra-high molecular weight polyethylene. *Biosurface and Biotribology*, 1(4):270–277, 2015. 2.3, 3.2.2

[70] de Kraker, Alex, van Ostayen, Ron A, Van Beek, A, and Rixen, Daniel J. A multiscale method modeling surface texture effects. *Journal of tribology*, 129(2):221–230, 2007. 2.3

[71] Vijayaraghavan, D and Keith, TG. An efficient, robust, and time accurate numerical scheme applied to a cavitation algorithm. *Journal of tribology*, 112(1):44–51, 1990. 2.4

[72] Fesanghary, M and Khonsari, MM. A modification of the switch function in the elrod cavitation algorithm. *Journal of Tribology*, 133(2):024501, 2011. 2.4

[73] Press, William H. *The art of scientific computing*. Cambridge university press, 1992. 2.4, 3.1

[74] Cherabi, Bilal, Hamrani, Abderrachid, Belaidi, Idir, Khelladi, Sofiane, and Bakir, Farid. An efficient reduced-order method with pgd for solving journal bearing hydrodynamic lubrication problems. *Comptes Rendus Mécanique*, 344(10):689–714, 2016. 4